NASA Technical Paper 1319

Experimental Evaluation of a Pilot Multinozzle-Duct Apparatus

Richard L. Puster

FEBRUARY 1979

NASA

NASA Technical Paper 1319

Experimental Evaluation of a Pilot Multinozzle-Duct Apparatus

Richard L. Puster
Langley Research Center
Hampton, Virginia

National Aeronautics
and Space Administration

**Scientific and Technical
Information Office**

1979

SUMMARY

A pilot multiple nozzle (multinozzle) and duct were built and tested at ambient enthalpy to evaluate the suitability of such apparatus for testing thermal protection system (TPS) panels mounted in the sidewalls of the duct downstream of the nozzle array. The flow field in the duct was complex: effects of wakes and shock waves from the nozzles dominated the flow field; the wakes continually mixed with the surrounding fluid; the boundary layer on the sidewalls of the duct was nonuniform; and near the exit of the duct the sidewall pressure variation was as much as 8.5 percent about the mean wall pressure. Starting loads on the duct walls were higher than those of a similar conventional nozzle and duct. It was concluded that the multinozzle-duct apparatus was not suitable for testing TPS panels, although the design and flow-field information should be of interest to designers of high-energy gasdynamic lasers.

INTRODUCTION

The disadvantages of nozzle designs for supersonic flow based on conventional two- or three-dimensional method-of-characteristics solution contours are well known, and include a distorted boundary layer on the sidewalls; shock-free flow at only one enthalpy level for a given contour; relatively large, long, expensive nozzles; and variable Mach number operation only with an expensive and an extensive jack contour changing system. The multiple-nozzle arrangement, or so-called multinozzle, was first used to develop supersonic flow in a duct in Germany in 1945 and in England in 1947 (ref. 1). The impetus for investigations of the multinozzle in the decade following World War II was the low cost of changing Mach number with another set of multinozzles and, hopefully, minimization of the undesirable secondary flows in the boundary layer. The wakes and shock system associated with the multinozzle, however, caused the flow to be so nonuniform that the configuration was considered unsuitable for any aerodynamic testing, and most investigations were discontinued for another decade or so. (See ref. 2.)

Two fairly recent applications have prompted a reevaluation of the multinozzle. One application is the gasdynamic laser (ref. 3), which uses the multinozzle to produce vibrational mode freezing of the gas molecules. The extremely short length of the multinozzle is well suited for this use; indeed, efficient high-power lasers are practical with this arrangement (ref. 4). Another potential use arises from the need for large, high enthalpy, variable Mach number facilities for testing thermal protection panels for hypersonic and reentry flight vehicles. The multinozzle possibly could be used for this purpose if the test panels were mounted in the wall of the duct downstream of the nozzle array. Such a test facility was proposed, and the pilot model apparatus described in this report was used to evaluate the suitability of a multinozzle-duct arrangement for testing large (about 0.6 by 1.0 m (2 by 3 ft)) flat thermal protection panels for the space shuttle and other future hypersonic

vehicles. The ambient-enthalpy-level test apparatus was a 1/6-scale model of the proposed test facility although the multinozzles array was 1/3 of full scale. Fluid-dynamic phenomena that exist at both ambient and elevated enthalpy levels were investigated with the pilot model. Areas of interest investigated were the internal flow field and its effect on sidewall flow fields.

Use of trade names or names of manufacturers in this report does not constitute an official endorsement of such products or manufacturers, either expressed or implied, by the National Aeronautics and Space Administration.

SYMBOLS

Values of physical quantities are given in both the International System of Units (SI) and U.S. Customary Units. Measurements and calculations were made in U.S. Customary Units.

A exterior nozzle contour (figs. 1 and 2)

B interior multinozzle contour (figs. 1 and 2)

E nozzle exit height (figs. 1 and 2), cm (in.)

ℓ exterior nozzle axial length (fig. 2), cm (in.)

M Mach number

N exponent, $\frac{V}{V_\infty} = \left(\frac{Z'}{\delta}\right)^{1/N}$

P pressure, kPa (lb/in^2)

r density defect in wake, $\frac{\rho_\infty - \rho_{(0)}}{\rho_\infty}$

S static pressure variation, $100\left(\frac{P}{P_m} - 1\right)$

T temperature, K (^oR)

t thickness of wake-producing object, cm (in.)

V velocity, km/sec (ft/sec)

W velocity defect, $\frac{V_\infty - V_{(0)}}{V_\infty}$

X	axial distance, cm (in.)
X_0	virtual origin of wake, cm (in.)
x'	axial distance along multinozzle (fig. 2), cm (in.)
Y	vertical distance from apparatus center line (fig. 1), cm (in.)
y'	vertical distance from nozzle center line to surface (fig. 2), cm (in.)
y^*	half nozzle-throat height
Z	spanwise distance from center of duct, cm (in.)
Z'	distance normal to sidewall, cm (in.)
γ	isentropic exponent
δ	boundary-layer thickness, cm (in.)
Θ	temperature defect, $\frac{T_{(0)} - T_\infty}{T_\infty}$
ρ	density, kg/m^3 (lbm/ft^3)

Subscripts:

a	ambient
c	plenum chamber
j	ejector
m	mean value
(0)	condition at center of the wake
t	stagnation or total
1	flow conditions ahead of shock
2	flow conditions behind shock
∞	free-stream conditions

Designations I and II refer to nozzle shock and trailing shock, respectively.

APPARATUS

Multinozzle-Duct Pilot Model

The test apparatus was a 1/3-scale model of a proposed full-scale tunnel. It consisted of three nozzles, used to expand the flow, followed by a constant-area duct. The basic geometry and dimensions of the model apparatus are shown in figure 1. The interior nozzle is 16.51 cm (6.500 in.) long and the exterior nozzles are 20.605 cm (8.112 in.) long and form part of the walls of the duct. The duct is 60.96 cm (24.00 in.) long with a width of 5.08 cm (2.00 in.) and a height of 15.24 cm (6.00 in.).

The full-scale apparatus was designed to operate from ambient enthalpy to an enthalpy level of 8.14 MJ/kg (3500 Btu/lb) and at total pressures of from 2 to 20 atmospheres. The design point for the nozzle contour was selected as an enthalpy level of 5.35 MJ/kg (2300 Btu/lb) and a total pressure of 10 atmospheres. The hot gas would be generated by the combustion of methane, air, and oxygen with the combustion products having a 20-percent-by-volume fraction of molecular oxygen. The equilibrium gas properties were calculated using the program of reference 5. These gas properties were then input into the computer program of reference 6 to calculate the nozzle contour.

The resultant contours scaled down by a factor of 3 are shown in figure 2. The axial coordinates are nondimensionalized by the length of the exterior nozzle (ℓ = 20.605 cm (8.112 in.)) and the vertical coordinates are nondimensionalized by the half nozzle-throat height (y^* = 0.1021 cm (0.0402 in.)). The subsonic contour of the interior nozzle is circular until the Mach number reaches 0.15 after which it is elliptical to the minimum-area location. From the minimum area to a nondimensional length X'/ℓ of 0.7764, the contour for both the interior nozzle and the exterior nozzle are the same. From this point to the exit, X'/ℓ = 0.8013, the contour B for the interior nozzle was determined by a hyperbolic spiral function. The exit wall angle for the interior nozzle was 1.0°. The blunt exit lip height and the shortened contour were dictated by cooling requirements at elevated enthalpy for the full-scale nozzle. The exterior nozzle has a full method-of-characteristics solution to its exit with an exit wall angle of zero. The design Mach number of the nozzles is 3.787 at an enthalpy level of 5.35 MJ/kg (2300 Btu/lb) and a total pressure of 10 atmospheres. The isentropic exponent γ varies from 1.129 at the throat region to 1.225 at the exit of the nozzle at the design enthalpy.

The complete model test apparatus is shown in figure 3. A sketch of the interior nozzle contour is also shown in figure 3 along with the location and shape of the gland side seal. After the flow exits from the constant-area duct, it enters a supersonic diffuser which has an adjustable Mach number ejector with a long mixing tube and subsonic diffuser. The duct was fitted with schlieren-quality glass so that the flow could be visualized and photographed.

The model apparatus, shown in figure 3 is uncooled, constructed mostly of aluminum, and operates using air at an ambient total enthalpy of 232.6 kJ/kg (100 Btu/lb) to 302.38 kJ/kg (130 Btu/lb). Air was used as the test gas because it was available in quantity and at high pressure. The use of another gas such as freon would have been a better simulation of the isentropic exponent

of the full-scale hot combustion products but freon or other gases were not available for this investigation. The total pressure range of the multinozzle-duct model was between 206.8 kPa (30 psia) and 2068 kPa (300 psia). Air was also used to operate the single stage variable Mach number ejector. The air was dried to a dew-point temperature of 206 K (371° R).

Instrumentation

Variations in the duct flow, generated by the multinozzle system, were recorded photographically using a single-path horizontal Z-light-path schlieren system that employed either a xenon light source, operated continuously or in a flash mode, or an air-gap spark light source. The xenon light source in the flash mode had a duration of 5 μsec while the duration of the air-gap spark light source was 0.2 μsec. Start-up of the multinozzle and duct was photographed with a high-speed camera operating at 5000 frames per second using the xenon light source in the continuous mode and with the flow visualization system set up as focused shadowgraph.

The flow field of the duct was surveyed with the probes shown in figure 4. Figure 4(a) shows pitot and static pressure probes for the vertical center-line flow-field survey. The probes were installed alternately with static and pitot tube orifices in the same location. A photograph of one of the pitot probes installed in the duct is shown in figure 4(b). The vertical position of the probe was indicated by a linear potentiometer while the pressure levels were measured with strain-gage pressure transducers. As seen in figure 4(c) the pitot probe used to survey the sidewall boundary layer had a smaller tip and different geometry to minimize flow disturbances. The time-invariant sidewall pressures were obtained from measurements made with flush orifices in steel blanks which replaced the glass windows. The locations of these orifices are listed in table I.

The transient starting pressure loads on the sidewalls of the duct were measured with four gages mounted flush with the inside wall of the duct. The gages used were unbonded flush diaphragm strain-gage pressure transducers. The gages were electrically isolated from the wall with Teflon[1] sleeves and gaskets. The response of these gages was flat to 1.2 kHz with very low sensitivity to vibratory accelerations. The gage output was filtered with an upper cutoff of 1.0 kHz and recorded on an FM tape recorder.

Test Conditions and Procedures

All of the tests were conducted at a constant total pressure of 586 kPa (85 psia) for the multinozzle flow with the air at low enthalpy levels depending upon ambient conditions, ranging from 290.8 kJ/kg (125 Btu/lb) to 302.4 kJ/kg (130 Btu/lb). The ejector was operated at the same enthalpy level and a total pressure of 3.00 MPa (435 psia). The ejector and multinozzle total pressures were such that the flow was supersonic in the first part of the mixing tube and

[1]Teflon: Trademark of E.I. du Pont de Nemours & Co., Inc.

all of the supersonic diffuser. The vertical (Y) traverses with both the pitot and static probes were made at constant total pressure and enthalpy. Measurements were taken at selected positions with the pitot pressure probe; then the static pressure probe was installed and the procedure repeated. Adequate time for the line and gage to reach a time-invariant value was assured. The flow was surveyed at the locations listed in table II. A similar procedure was also used for the boundary-layer surveys except that the static pressure was measured only at the wall. The locations of the boundary-layer flow surveys are also listed in table II.

RESULTS AND DISCUSSION

Flow-Field Visualization

The flow produced by the multinozzle is complex with two systems of flow disturbances, shock waves and wakes, originating from the exit region of the nozzles as shown in figure 5. This photograph shows the boundary layer of the nozzle in the exit region with its relatively thick turbulent structure apparent. Near the exit of the nozzles is a shock wave which is designated as I. This shock wave is primarily a result of using an arbitrary curve to turn the flow from a wall angle of 3.5° to 1.0°, and to a lesser extent, using a test medium (air) with a substantially different isentropic exponent than that of combustion products at the high design enthalpy level of 5.35 MJ/kg (2300 Btu/lb). Close examination of the photograph of the flow at the exit of the nozzle shows a pronounced expansion terminated by a shock wave. The strong lip shock wave can be seen followed by the neck region and the trailing shock wave which is designated as II. By examining the region immediately downstream of the nozzle exit, the near wake and wake neck can be seen. Immediately downstream of the neck region the growth and structure of the wake can be seen. The visual appearance of the wake, the growth rate, and the herringbone-like pattern of density variations indicate that the wake is turbulent. Immediately downstream of shock wave II, and extending around the edges of the wake, there is a strong expansion region with the strength of the expansion decreasing with axial length as the wake width (or height) increases. The process attentuates the strength of the shock wave II. The flow field in the near wake and the region downstream are complex; a more complete and thorough discussion of this type of flow field may be found in reference 7.

The near flow field in the exit region and the flow in the duct from $X = -2.16$ cm (-0.85 in.) to $X = 25.65$ cm (10.10 in.) are shown in the schlieren photograph of figure 6; also the four oblique shocks from each nozzle as well as the two wakes. It is also evident from figure 6 that there are no visible shock waves from the exterior contours. Thus the type I shocks from the interior contours could be eliminated by using a full method-of-characteristics solution to the end of the nozzle. In the shadowgraph (air-gap spark light source) of the flow field from $X = 12.95$ cm (5.10 in.) to $X = 26.67$ cm (10.50 in.), the structure of the wakes and boundary layer can be seen in greater detail. In addition to the wakes from the interior nozzle and boundary layer on the bottom and top walls, other flow-field disturbances are visible in figure 7. The flow region at the center of each nozzle contains regions of large-scale density variations but of much lower strength than the wakes. These disturbances are

probably caused by a slight leak of high pressure air past the nozzle seals in the throat region resulting in jet-mixing regions. While these disturbances may be of minor consequence at the location shown in figure 7, the flow in the downstream regions was increasingly affected in an adverse manner by these disturbances.

Figure 8 is a shadowgraph (air-gap spark light source) of the flow field from X = 32.38 cm (12.75 in.) to X = 49.40 cm (19.45 in.). The density variations are much less pronounced than in previous flow-field photographs. The wakes, nozzle flow-field disturbances from jet mixing, and the boundary layers at the top and bottom of the duct can be observed. However, the density variations caused by the shock waves are not visible unless horizontal knife edge, continuous-xenon-source schlieren flow visualization is used.

Multinozzle-Duct Flow Field

The flow field shown in figures 5 to 8 is characterized by two major disturbances - shock waves and wakes. The flow within each nozzle from the subsonic approach to the supersonic exit is the same as that of a conventional supersonic nozzle. Using the nozzle design procedure described for the interior nozzle and exterior nozzle, weak compression waves are present but are insignificant compared to the type I shock wave emanating from the interior nozzles. This shock wave can be eliminated by using a full method-of-characteristics solution contour. Another design defect was the O-ring gland seal, as seen in figure 3, used to seal the high pressure subsonic air from the low pressure supersonic flow. The seal should have extended to the edge of the contour, which would have eliminated the jet-mixing wake that occurred. The trailing-shock-wave strength (type II) would be minimized as the exit-lip heights were decreased; however, the wakes would always be present. Other multinozzle designs and evaluations are described in references 8 to 10.

Duct Free-Stream Flow Properties

Duct free-stream flow-field surveys.- The flow field within the duct is dominated by the disturbances that originate from the multinozzle. The flow field was surveyed at five axial stations to define its characteristics including types of shock waves and wakes. Vertical (Y) measurements of pitot pressure, normalized by the plenum chamber total pressure, for the five axial positions surveyed are presented in figure 9. From figure 9 the presence of the wakes can easily be seen by the much lower pitot pressures in the wake flow regions. The location and effect of the shock waves on the pitot-pressure distribution is not as pronounced; hence, their position was determined by xenon continuous-mode-source schlieren photographs of the flow field. The positions and types of shock waves are easily identified and are indicated in figure 9. Static pressures, also normalized by the plenum chamber pressure for the same axial stations, are presented in figure 10. Again, the shock waves are identified for easy reference. By assuming that the total temperature was constant, calculations were made, using measured pressures, of Mach number, velocity, and density at these same axial stations. These quantities are presented in

figures 11 to 13. The trends shown in these figures are easier to see; the Mach number, velocity, and density in the wake regions produced by the multinozzle are lower than the corresponding values in regions outside the wakes. The differences between the Mach number and velocity in the wake and in areas surrounding the wakes are large with the difference decreasing with downstream position. The difference in density, between that of the wake and surrounding flow areas, is less pronounced; but the trend, with increasing axial position, is the same as the other flow parameters. The shock waves and their effect on the flow are seen to be of decreasing consequence with increasing axial position. The apparatus of reference 2 has about the same Mach number and a similar Reynolds number as the apparatus of this investigation so that the detailed description given in reference 2 of the significance of variations similar to those presented in figures 9 to 13 is valid for the present results. Hence, a detailed description is not given in this paper.

Trends and comparisons with other data of the free-stream flow.- The variation in Mach number along the duct is shown in figure 14 for the centers of both the free-stream flow and the wake flow, $Y = 2.54$ cm (1.00 in.) and $Y = -2.54$ cm (-1.00 in.), respectively. The Mach number of the free-stream flow shown in figure 14 drops rapidly near the beginning of the duct because of the shock waves generated by the multinozzle. After a length, $X/E = 3.0$, the decrease is very gradual. The wake center-line Mach number increases continually with axial distance, although the rate of increase decreases with length. For example, near the exit of the duct ($X/E = 11.66$), the wake Mach number has reached 3.26 while the free-stream Mach number has dropped to 4.10.

The change in wake strength is plotted in terms of pitot pressures in figure 15 as a function of nondimensional axial distance X/E. The pitot pressure at the center of the wake $P_{t,2,(0)}$ divided by the local free-stream pitot pressure $P_{t,2,\infty}$ increases with axial length. Analogous to defining the edge of a boundary layer, the wake width was defined as the distance between the locations at which the Mach number, temperature, and pitot pressure are 95 percent of free-stream conditions. The width of the wake in the X-Y plane as a function of axial distance is plotted in figure 16, which shows that the growth of the wake is parabolic. Figures 14 to 16 indicate that the wake is continuously growing at the expense of the surrounding fluid. Thus, if the trends continue with axial distance, as indicated by the experimental data, the wake would continue to exchange momentum and energy with the surrounding fluid, until the identity of the wake was lost.

The velocity defect W is plotted as $1/W^2$ as a function of the nondimensional axial distance in figure 17. The axial distance is normalized by $(X - X_o)/E$ for the multinozzle of the present investigation and also for the investigation of reference 2. In both cases E is the nozzle exit height. The virtual origin of the wake X_o, obtained by plotting X against $1/W^2$, is defined as the X-intercept. Other data from references 11 and 12 are plotted in figure 17; for these data the distances were normalized by the thickness t of the wake-producing object. By using the data of figure 17, the velocity defect for duct lengths longer than those investigated can be obtained by simple extrapolation of the plotted curve or by a first-order curve fit of the data. By using this technique, which is justified in reference 12, it was

found that the wake center-line velocity would reach 95 percent of the free-stream velocity at a nondimensional length X/E of 18.3.

The use of similar techniques were set forth for the density defect r and the temperature defect Θ in reference 12. However, these techniques do not yield a linear relationship of $1/r^2$ and $1/\Theta^2$ with axial distance unless data are used for the far-field wake only. Part of the reason for the nonlinear behavior of the density defect is the axial variation of static pressure which was observed in references 2 and 12 and in the present study. Therefore, since the data from the present study were in the nonlinear region of the density- and temperature-defect curves, extrapolation to longer distances than those measured would be invalid.

Usually, as reported in reference 13, pressure disturbances such as shock waves enhance the mixing process of the wake. In addition, other pressure gradients such as those caused by boundary-layer growth can have an effect on the phenomena of the mixing of the wake with the surrounding fluid. However, the wakes generated by the multinozzle of reference 2 decay to a certain point, and approach a nearly constant value of wake strength as indicated by pitot pressure and Mach number. In reference 2 at an axial length X/E of about 18 (E in ref. 2 is 2.54 cm (1.00 in.)) the ratio of wake center-line pitot pressure to that of the local free stream reaches a value of 0.58, and the wake Mach number reaches a value of 3.48 which is 80 percent of the free-stream Mach number; thereafter there is little or no change in the above parameters with axial distance. However, in this investigation the wake decay neither ceased nor asymptotically approached a constant value of wake strength; this variation was shown in figures 15 and 17. Nevertheless, the information presented about the flow field in the duct should be of considerable interest to designers of high-energy gasdynamic lasers.

Duct-Sidewall Pressures

Pressures were measured on both duct sidewalls with static pressure orifices located at 14 vertical locations between $Y = 0.0$ and ± 7.62 cm (± 3.00 in.) and 13 axial locations, as listed in table I. Since the flow field was symmetrical only the sidewall pressures between the center line and the bottom of the duct are presented. Static pressures on the walls, normalized by the plenum-chamber pressure, are plotted in figure 18, as functions of vertical distance at each axial location; the position of the shock waves are also given on each plot where schlieren flow visualization was possible. Since the free-stream static pressures were measured at five axial locations, these data are also plotted for comparison of sidewall pressures with free-stream pressures in the center of the duct. The static pressure variation S about the mean local wall (or free-stream) pressure is also plotted in figure 18. Examination of figure 18 gives insight into the variation of static pressures on the duct sidewalls, and five comparisons of sidewall pressures with the static pressures at the center of the duct in a plane parallel to the duct sidewalls. Near the exit of the multinozzle and the beginning of the duct, large variations in static pressure are evident (see figs. 18(a) to 18(d)). The variation in pressure on the duct sidewalls is as high as 20 percent about the mean local wall pressure

at X/E = 0.282 and decreases to 15 percent or less at X/E = 3.25. The free-stream pressure variations are more pronounced with variations as high as 28 percent at X/E = 3.25. Examination of further downstream locations, X/E = 4.13 to 7.16 (figs. 18(e) to 18(h)), reveals lower amplitude pressure variations that are usually 10 percent or below unless the measurement is in close proximity to a shock wave; then the variation may be as great as 15 percent. Figures 18(i) to 18(m), X/E = 8.25 to 11.66, show pressure variations usually less than 10 percent on the sidewalls although the free-stream flow has a pressure variation well above 10 percent at X/E = 9.16. The last position measured, X/E = 11.66 (fig. 18(m)), shows a pressure variation of 8.5 percent about the mean local wall pressure on the sidewalls and up to 10 percent in the free stream.

Variations of both the mean wall static pressure and the wall static pressure beneath the wake center line divided by the plenum chamber total pressure $P_{t,c}$ with axial distance X/E are shown in figure 19. The mean wall pressure increases with axial distance, and the wall pressure below the wakes is usually greater than a least-square curve fit of the mean wall pressure and is, also, for the most part greater than the mean local wall pressure. Thus, in addition to the axial positive pressure gradient, there is a vertical positive spanwise gradiant on the walls between the area under the wakes and wake-free area. This gradiant will affect the sidewall boundary layer.

Duct-Sidewall Boundary Layer

The nonuniform boundary layer at the exit of a conventional two-dimensional nozzle is well known. (See refs. 14 and 15.) The use of a short nozzle such as the multinozzle would lead to the same nonuniform boundary layer, but the boundary layer would be thinner because the nozzle could be much shorter. The boundary-layer thickness on the multinozzle used in this investigation was calculated using the method of reference 16; the calculated boundary-layer thickness at the exit of the multinozzle was only 15.6 percent of the nozzle exit height. Thus, although the boundary layer may be very nonuniform, the effect of the boundary layer on the inviscid flow has been minimized. The effect of the wakes and complex flow field in the duct downstream of the multinozzle, however, was not known. In order to determine whether or not the boundary layer was uniform, relatively far downstream of the nozzle array, one axial position (X/E = 9.16) and two vertical positions (one at the center line, Y = 0, and one below a wake, Y = -2.54 cm (-1.00 in.)) were surveyed.

The Mach number distribution is plotted in figure 20 as a function of Z', the distance normal to the sidewall. Figure 21, shows the ratio of local to free-stream velocity plotted for the same two locations as a function of Z' divided by the boundary-layer thickness δ. As can be seen in figures 20 and 21 the boundary layer is not uniform. The boundary layer at the center line reaches a plateau of Mach number at about 1.0 cm (0.394 in.) in figure 20; the Mach number at this point is only 2.58 and the velocity is 582 m/sec (1910 ft/sec) from figure 21. At this same distance Z' under the wake from figures 20 and 21, the Mach number is 3.48 and velocity is 651 m/sec (2135 ft/sec). The Mach number and velocity at the center line increase again to their final level at near the midpoint of the duct (Z = 0).

The plateaus in Mach number and velocity are most likely caused by the sidewall-nozzle seal leak that caused the jet-mixing region that was observed previously in figures 7 and 8. Further examination of figure 21 reveals that the flow field on the sidewall outside the wake has viscous effects present for over twice the boundary-layer thickness of the area under the wake. It was shown in figures 18 and 19 that there was a pressure gradient between the area on the sidewalls under the wakes (caused by the multinozzle) and the adjacent areas not influenced by these wakes; and, that the pressure gradient was usually positive. In addition to the effects caused by the nozzle-seal leaks, shock waves, and pressure gradients, the boundary layer under a wake would experience a mass loss and momentum gain relative to the surrounding fluid with the effect decreasing with distance. The net effect of these phenomena would be to produce a very nonuniform and complex boundary layer along the duct sidewalls. Additional survey positions would have revealed a more complete picture of the boundary layer, but for sidewall panel testing it is sufficient to know that the boundary layer is nonuniform.

Flow Start Characteristics and Transient Wall Loads

The flow start process of a conventional nozzle and the loads associated with the process are described in references 17 and 18.

The starting process of the multinozzle is shown in the shadowgraphs of figure 22. In the starting sequence shown, the time and total pressure increase with numerical assignment of each photograph; however, the magnitude of the total pressure and time associated with each photograph was not measured. Usually the interior nozzle starts first with the exterior nozzles starting slightly later. The starting of the duct can be seen in sequence photograph (8); the flow separates from both the top and bottom walls with the fully developed supersonic flow terminated by a strong oblique shock wave on the top and bottom walls. The shock system is usually not symmetric. The flow downstream of the oblique shock is supersonic and at a lower Mach number; downstream of this region is a constant-pressure shear layer separating the subsonic flow from the mixed-flow supersonic region. The wake flow from the lower nozzle decelerates through a strong curved oblique shock. The interaction of the top oblique shock with the flow from the top nozzle consists of a number of strong oblique shocks interacting with the top-nozzle shocks and developing wake. This complex flow system moves quickly down the duct and in sequence photograph (9) of figure 22 the flow is seen to be completely started.

The experimentally determined operating envelope for the multinozzle wind tunnel is shown in figure 23 which shows the minimum combination of plenum-chamber total pressure and ejector total pressure, normalized by ambient pressure, necessary to start the tunnel and the minimum combination necessary for keeping the flow started (unstart boundary). Calculation of the operational boundaries can be made using the methods outlined in reference 19 and a good description of the starting and operating limits of supersonic wind tunnels using auxiliary air injection downstream of the test section may be found in reference 20. The start and unstart pressure transients on the duct sidewalls were measured with the single-stage variable Mach number ejector set to operate at a Mach number of 4.33; during the starting loads tests, the mean ejector

total pressure was 2930 ± 62 kPa (425 ± 9 psia). The total pressure required for starting the duct was 483 ± 21 kPa (70 ± 3 psia) and the minimum run pressure was 324 ± 6.9 kPa (47 ± 1.0 psia); these operating points are shown on figure 23. The flow start and unstart loads are about the same and are 20.0 ± 3.45 kPa (2.9 ± 0.50 psia). Another wind tunnel was built using a conventional nozzle with the same duct, supersonic diffuser, ejector, mixing tube, and subsonic diffuser as those of the multinozzle-duct apparatus evaluated in this report. The starting pressure transients on the walls of that duct were considerably lower than the duct walls of the multinozzle at 4.83 ± 2.07 kPa (0.7 ± 0.30 psia). The design pressure loading for lightweight metallic reentry thermal-protection-system structures is usually 14 kPa (2 psia) or less. (See p. 13 of ref. 21.) Thus, the starting loads imposed on the panel by the multinozzle-duct apparatus may be too high to be acceptable.

CONCLUDING REMARKS

A multiple nozzle array (multinozzle) of three nozzles with an attached duct was tested at ambient enthalpy and a total pressure of 5.78 atmospheres. The purpose of the tests was to evaluate the suitability of such an apparatus for testing thermal protection systems (TPS) panels for hypersonic and reentry vehicles mounted in the sidewall of the duct downstream of the nozzle array. Pitot and static pressure measurements and photographs were made of the flow field in the duct; and measurements on the sidewalls of the duct were made that included the sidewall boundary layer, the pressure distribution, and the transient loads caused by starting the tunnel.

The investigation of the free-stream flow field revealed a very complex flow field dominated by wakes from the multinozzle and, to a lesser extent, shock waves from the same nozzles. The wakes from the multinozzle were shown to be continually mixing with the surrounding fluid. The effect of the wakes and shocks on the duct sidewalls was pronounced, especially in the beginning of the duct. Near the exit of the duct the variation of the duct sidewall pressure had decreased to 8.5 percent about the mean local wall pressure. The boundary layer on the sidewall of the duct was nonuniform. The boundary-layer thickness under the wakes was less than one-half that of the boundary layer in the region near the center line near the duct exit. Transient pressure loads (20.0 ± 3.45 kPa (2.9 ± 0.50 psia)) caused by starting or unstarting the flow were too high for lightweight TPS panels. From these tests it was concluded that the multinozzle-duct apparatus would not be suitable for testing TPS panels. However, the information presented about the design of the apparatus and the flow field in the duct should be of considerable interest to designers of high-energy gasdynamic lasers.

Langley Research Center
National Aeronautics and Space Administration
Hampton, VA 23665
October 24, 1978

REFERENCES

1. Royle, J. K.; Bowling, A. G.; and Lukasiewicz, J.: Calibration of Two Dimensional and Conical Supersonic Multi-Nozzles. Rep. No. Aero. 2221, S.D.23, British R.A.E., Sept. 1947.

2. Wagner, Jerry L.: A Cold Flow Field Experimental Study Associated With a Two-Dimensional Multiple Nozzle. NOLTR 71-78, U.S. Navy, July 1, 1971.

3. Gerry, Edward T.: Gasdynamic Lasers. SPIE J., vol. 9, no. 2, Dec.-Jan. 1971, pp. 61-70.

4. Emmet, John L.: Frontiers of Laser Development. Phys. Today, Mar. 1971, pp. 24-31.

5. Kendall, Robert M.: An Analysis of the Coupled Chemically Reacting Boundary Layer and Charring Ablator. Part V - A General Approach to the Thermochemical Solution of Mixed Equilibrium-Nonequilibrium, Homogeneous or Heterogenous Systems. NASA CR-1064, 1968.

6. Johnson, Charles B.; Boney, Lillian R.; Ellison, James C.; and Erickson, Wayne D.: Real-Gas Effects on Hypersonic Nozzle Contours With a Method of Calculation. NASA TN D-1622, 1963.

7. Berger, Stanley A.: Laminar Wakes. American Elsevier Pub. Co., Inc., 1971.

8. Reshotko, Eli; and Haefeli, Rudolph C.: Investigation of Axially Symmetric and Two-Dimensional Multinozzles for Producing Supersonic Streams. NACA RM E52H28, 1952.

9. Gould, Lawrence I.: Preliminary Investigation of the Supersonic Flow Field Downstream of Wire-Mesh Nozzles in a Constant-Area Duct. NACA RM E51F25, 1951.

10. Lange, A. H.; and Walter, L. W.: Pressure and Temperature Measurements of the Flow Produced by a 12 × 12 cm Grating Nozzle. NAVORD Rep. 2678, U.S. Navy, Jan. 28, 1953.

11. Demetriades, A.: Compilation of Numerical Data on the Mean Flow From Compressible Turbulent Wake Experiments. Publ. No. U-4970, Aeronutronic Div., Philco-Ford Corp., Oct. 1, 1971.

12. Demetriades, Anthony: Turbulent Mean-Flow Measurements in a Two-Dimensional Supersonic Wake. Phys. Fluids, vol. 12, no. 1, Jan. 1969, pp. 24-32.

13. Ferri, Antonio: A Critical Review of Heterogeneous Mixing Problems. Astronaut. Acta, vol. 13, nos. 5 & 6, Aug. 1968, pp. 453-465.

14. Talbot, L.: A Mach 3.106 Two-Dimensional Adjustable Nozzle for Low Density Flow (No. 10 Nozzle). Rep. No. HE-150-120 (Contract NAw-6287), Inst. Eng. Res., Univ. of California, Feb. 18, 1954.

15. Haefeli, Rudolph C.: Use of Fences To Increase Uniformity of Boundary Layer on Side Walls of Supersonic Wind Tunnels. NACA RM E52E19, 1952.

16. Anderson, E. C.; and Lewis, C. H.: Laminar or Turbulent Boundary-Layer Flows of Perfect Gases or Reacting Gas Mixtures in Chemical Equilibrium. NASA CR-1893, 1971.

17. Bull, G. V.: Starting Processes in an Intermittent Supersonic Wind Tunnel. UTIA Rep. No. 12, Univ. of Toronto, Feb. 1951.

18. Robinson, M. L.; and Landers, E. R. A.: Starting Loads in Supersonic Wind Tunnels and Some Methods for Their Alleviation. Rep. HSA 22, Weapons Res. Establ., Australian Def. Sci. Serv., May 1967.

19. Spiegel, Joseph M.; Hofstetter, Robert U.; and Kuehn, Donald M.: Applications of Auxiliary Air Injectors to Supersonic Wind Tunnels. NACA RM A53I01, 1953.

20. Hunczak, Henry R.; and Rousso, Morris D.: Starting and Operating Limits of Two Supersonic Wind Tunnels Utilizing Auxiliary Air Injection Downstream of the Test Section. NACA TN 3262, 1954.

21. Black, W. E.; et al.: Evaluation of Coated Columbium Alloy Heat Shields for Space Shuttle Thermal Protection System Application. Volume I. Phase 1 - Environmental Criteria and Material Characterization. NASA CR-112119, 1972.

TABLE I.- SIDEWALL-PRESSURE-ORIFICE LOCATIONS

Vertical locations Y/E	Axial locations X/E
0	0.282
.125	1.375
.250	2.282
.375	3.250
.438	4.13
.500	4.78
.563	6.25
.625	7.16
.750	8.25
.875	9.16
1.000	10.25
1.125	11.00
1.250	11.66
1.375	

TABLE II.- FLOW-FIELD SURVEY LOCATIONS

Vertical survey locations (Z = 0)	
Y/E	X/E
-1.375 to 1.375 (in increments of 0.063)	1.38 3.25 7.16 9.16 11.66

Boundary-layer survey locations		
X/E	Y/E	Z'
9.16	0 -.5	0.051 cm (0.02 in.) to 2.54 cm (1.00 in.) (in increments of 0.064 cm (0.025 in.) or 0.127 cm (0.05 in.) (depending on position))

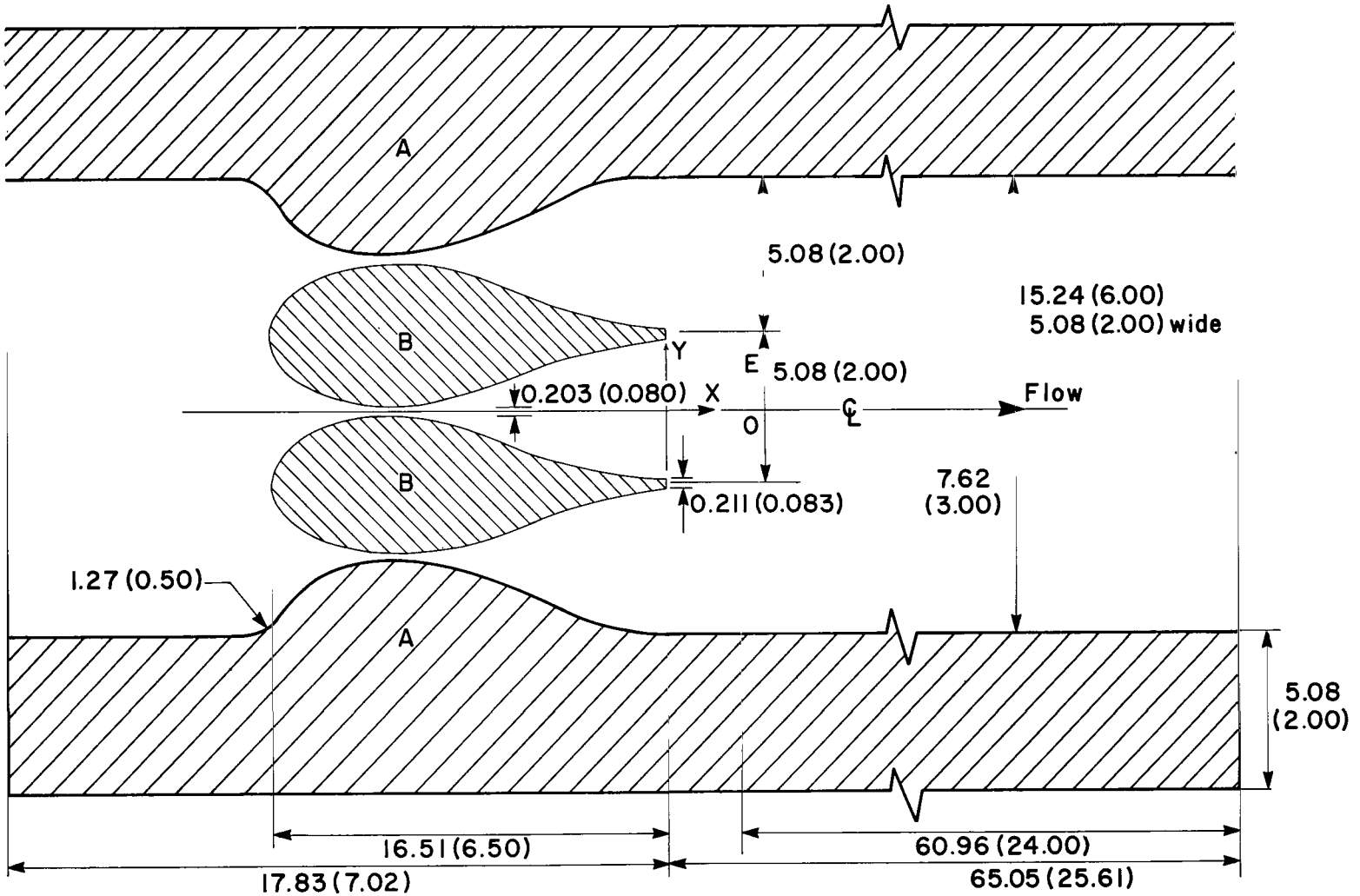

Figure 1.- Schematic drawing of multinozzle-duct assembly. All dimensions are in cm (in.).

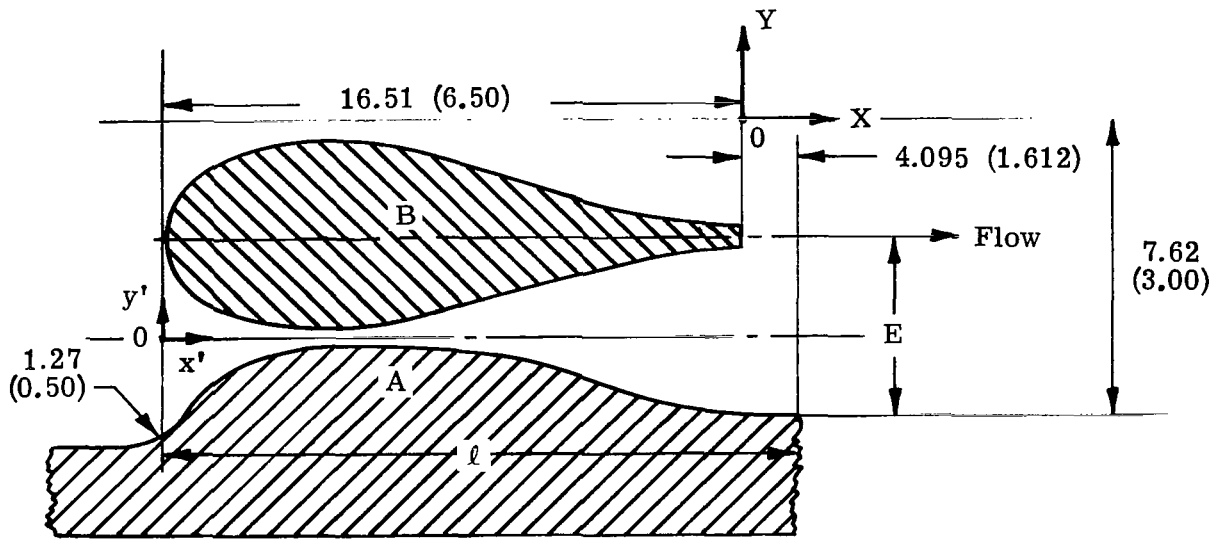

ℓ = 20.605 (8.112)

y* = 0.1021 (0.0402)

Nozzle contour A			
x'/ℓ	y'/y*	x'/ℓ	y'/y*
0.0000	24.8756	0.5200	18.2488
.0105	14.9080	.5463	19.0672
.0580	4.0199	.5720	19.7985
.0858	1.8152	.5972	20.4527
.1005	1.2687	.6220	21.0373
.1130	1.0647	.6463	21.5647
.1192	1.0100	.6702	22.0348
.1233	1.0000	.6937	22.4552
.1479	1.0174	.7167	22.8308
.1855	1.1219	.7394	23.1617
.2066	1.2761	.7617	23.4577
.2180	1.5896	.7837	23.7189
.2267	1.9602	.8054	23.9453
.2449	3.1244	.8267	24.1443
.2641	4.5274	.8478	24.3134
.2930	6.7015	.8685	24.4577
.3354	9.7189	.8889	24.5771
.3703	11.8209	.9091	24.6766
.4093	13.8458	.9291	24.7537
.4378	15.1517	.9482	24.8085
.4519	15.7488	.9681	24.8483
.4796	16.8358	1.0000	24.8756

Nozzle contour B	
x'/ℓ	y'/y*
0.7764	23.6343
.7801	23.6766
.7837	23.7114
.7889	23.7612
.7910	23.7761
.7932	23.7935
.7951	23.8060
.7963	23.8134
.7982	23.8234
.7994	23.8308
.8013	23.8383

Note: Nozzle contours are same except as listed.

Figure 2.- Nozzle coordinates. All dimensions are in cm (in.).

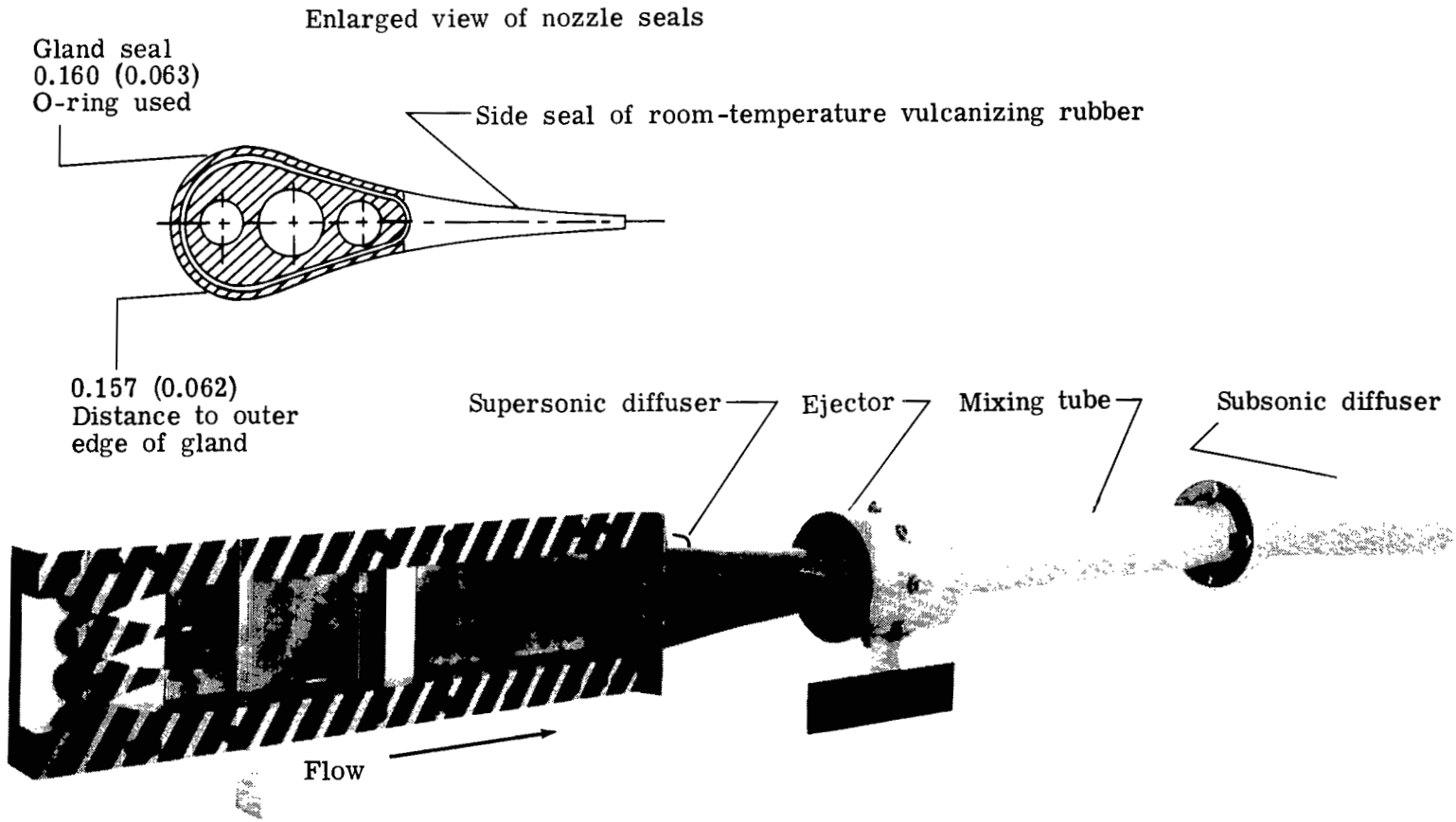

Figure 3.- Multinozzle-duct test apparatus. All dimensions are in cm (in.).

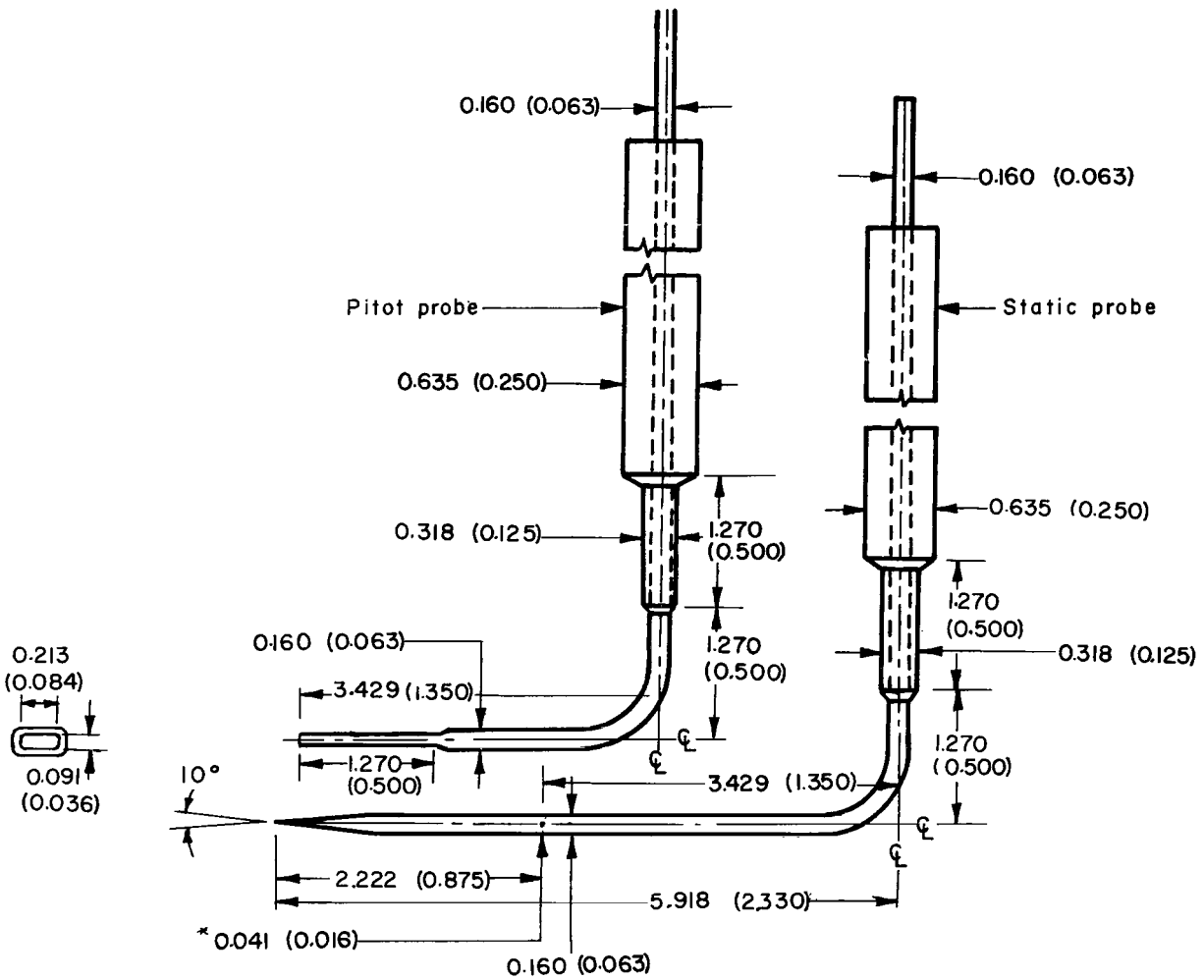

* 4 equispaced orifices 0.079 (0.031) stagger

(a) Pitot and static probes used for vertical (Y) survey.

Figure 4.- Flow-field survey probes and apparatus. All dimensions are in cm (in.).

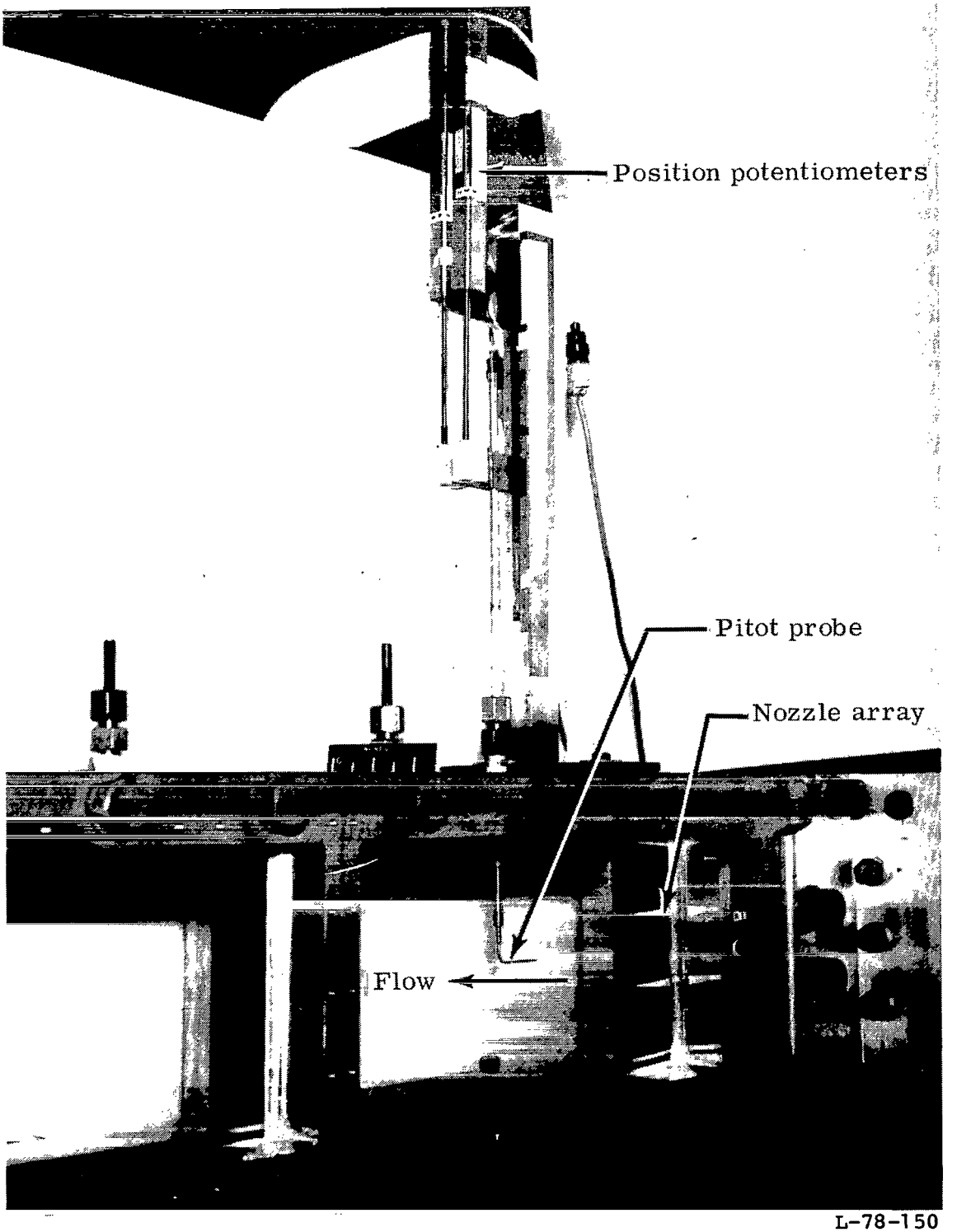

(b) Vertical (Y) traverse arrangement.

Figure 4.- Continued.

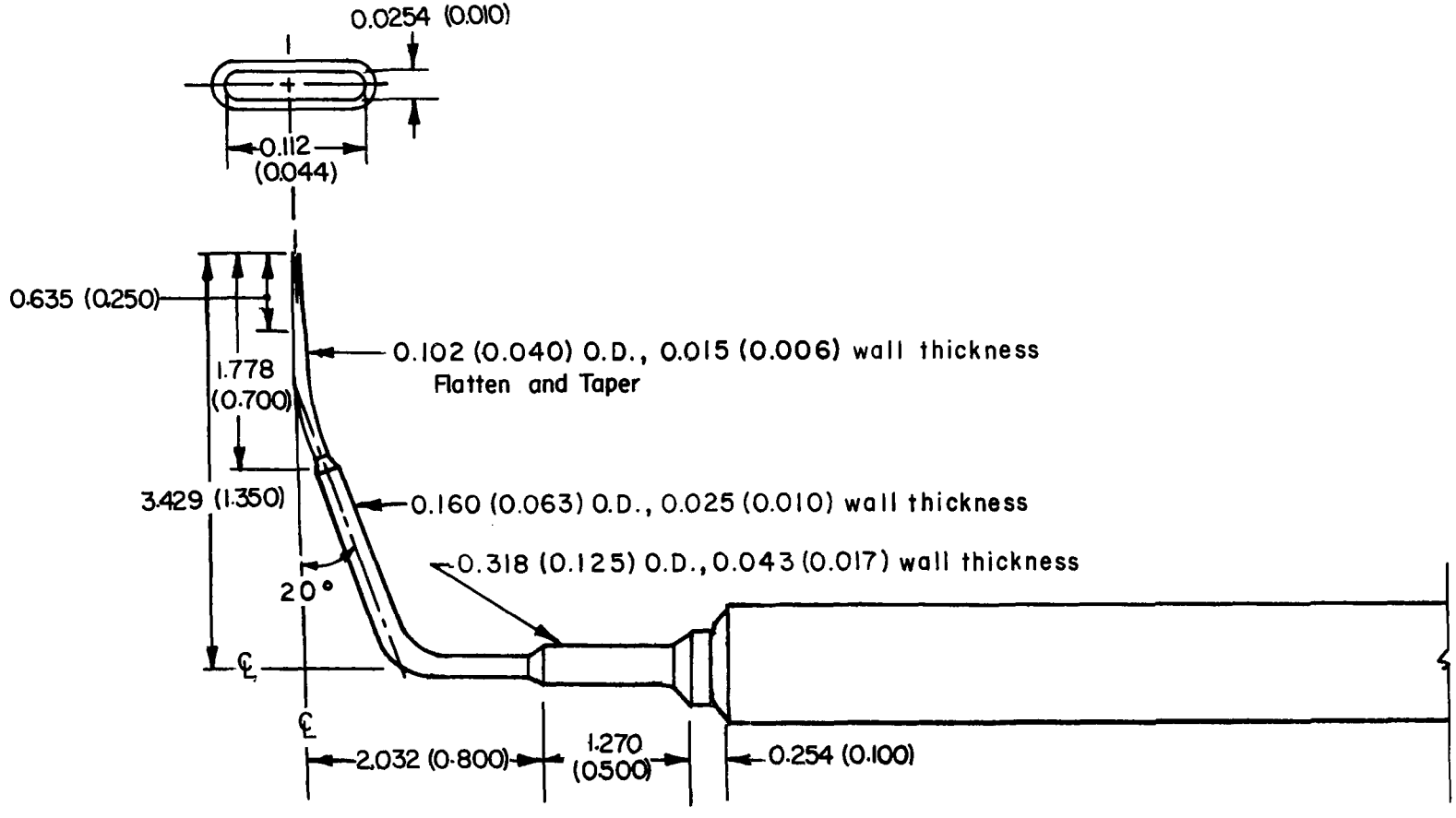

(c) Boundary-layer pitot probe.

Figure 4.- Concluded.

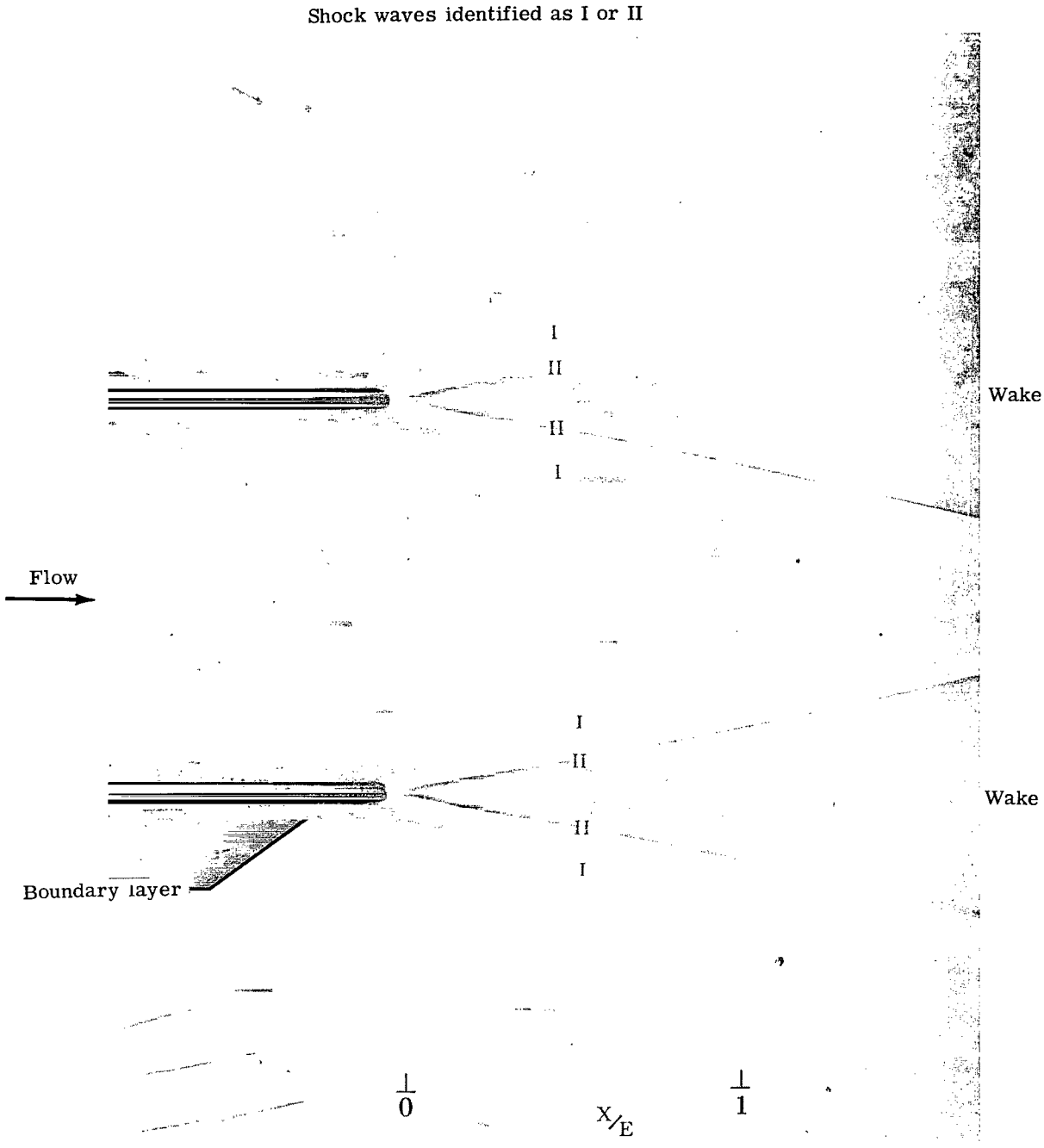

Figure 5.- Shadowgraph of nozzle exit flow, air-gap spark source. -3.68 cm (-1.45 in.) ≦ x ≦ 7.75 cm (3.05 in).

Shock waves identified as I or II

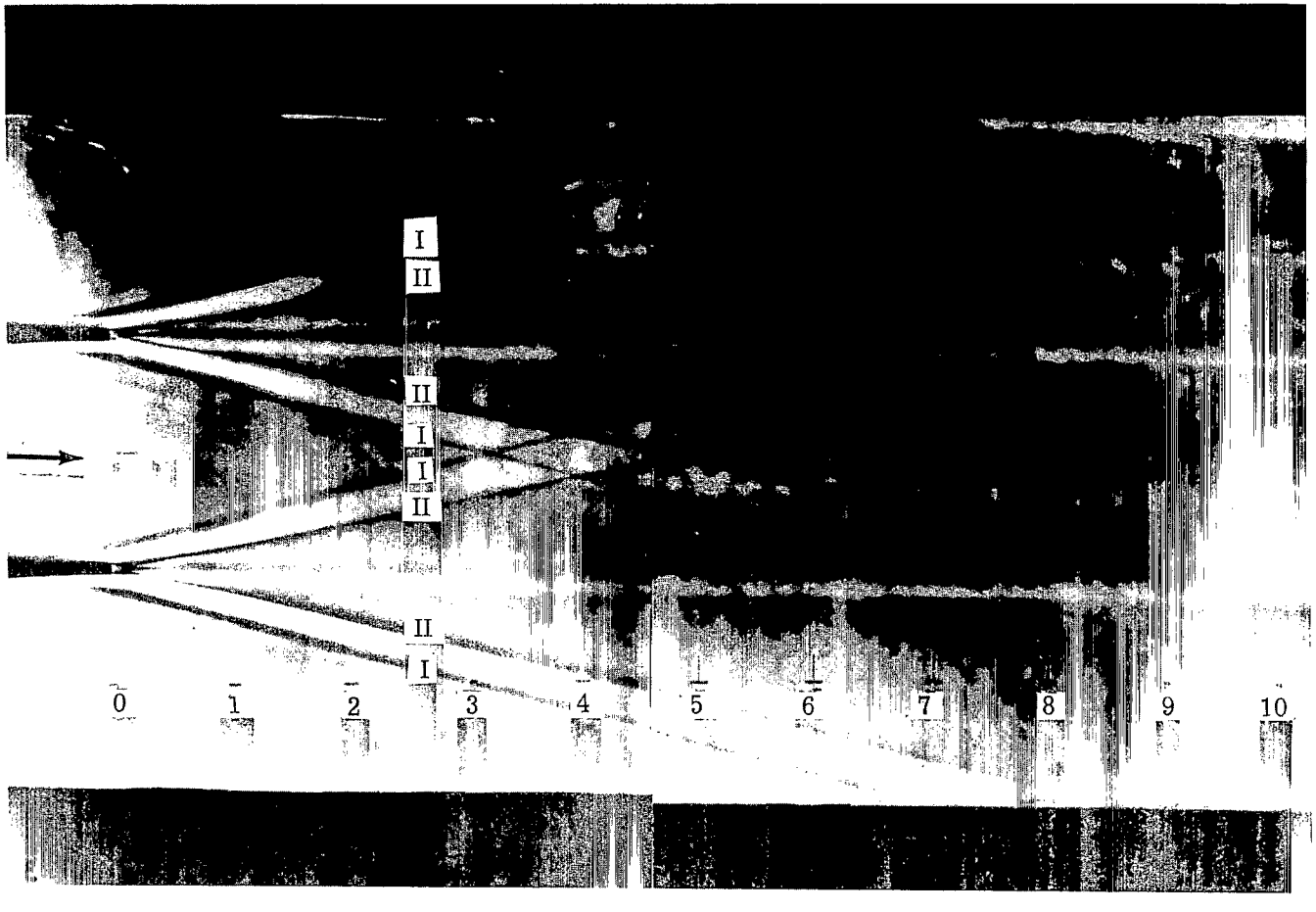

2 X/E

Figure 6.- Vertical knife edge schlieren photograph of duct flow, xenon light source, showing shock waves. -2.16 cm (-0.85 in.) ≦ X ≦ 25.65 cm (10.10 in.). L-78-151

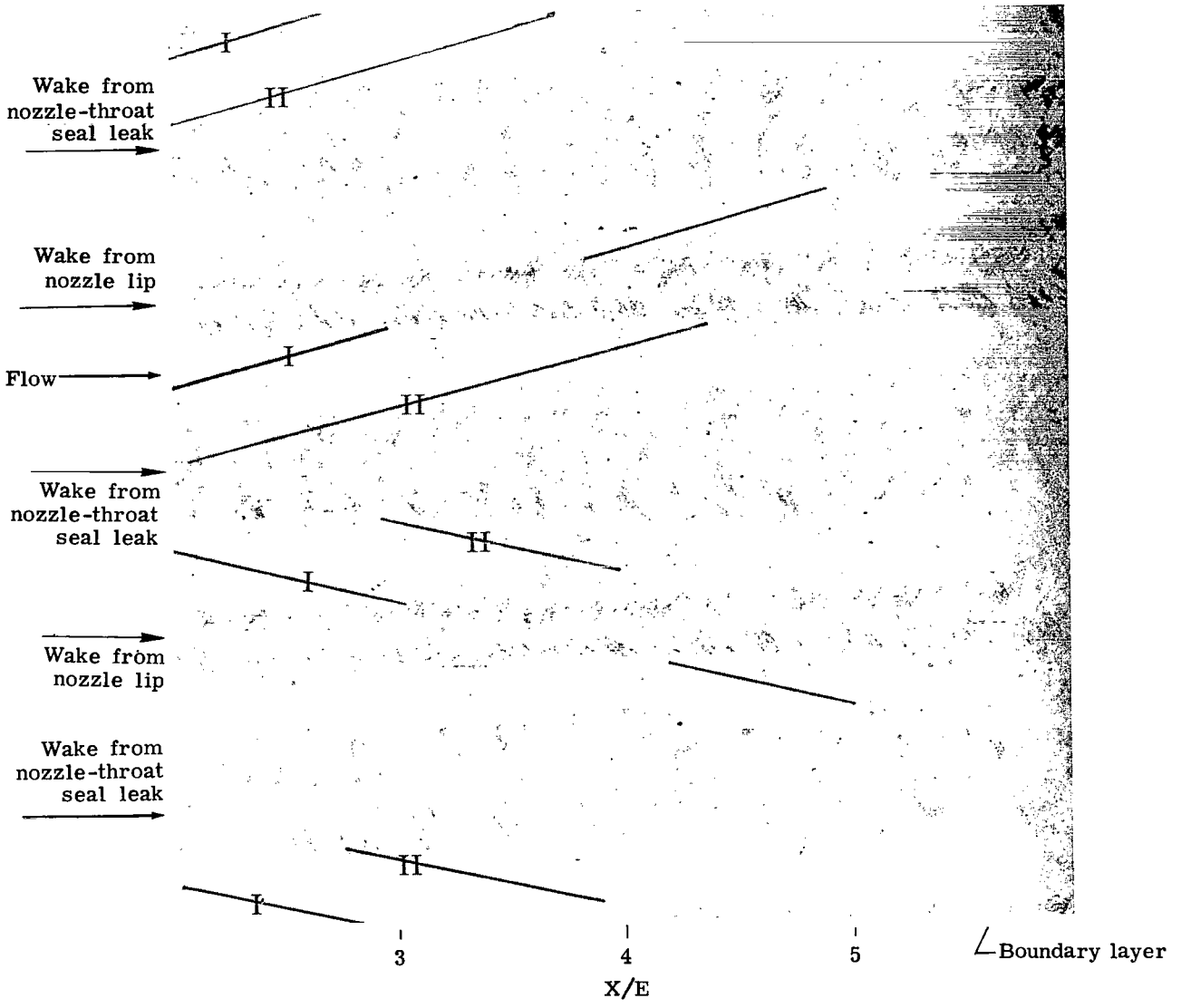

L-72-4370.1

Figure 7.- Shadowgraph of duct flow, air-gap spark source, emphazing wake flow. 12.95 cm (5.10 in.) ≦ X ≦ 26.67 cm (10.50 in.). Shock-wave positions are drawn on photograph and identified.

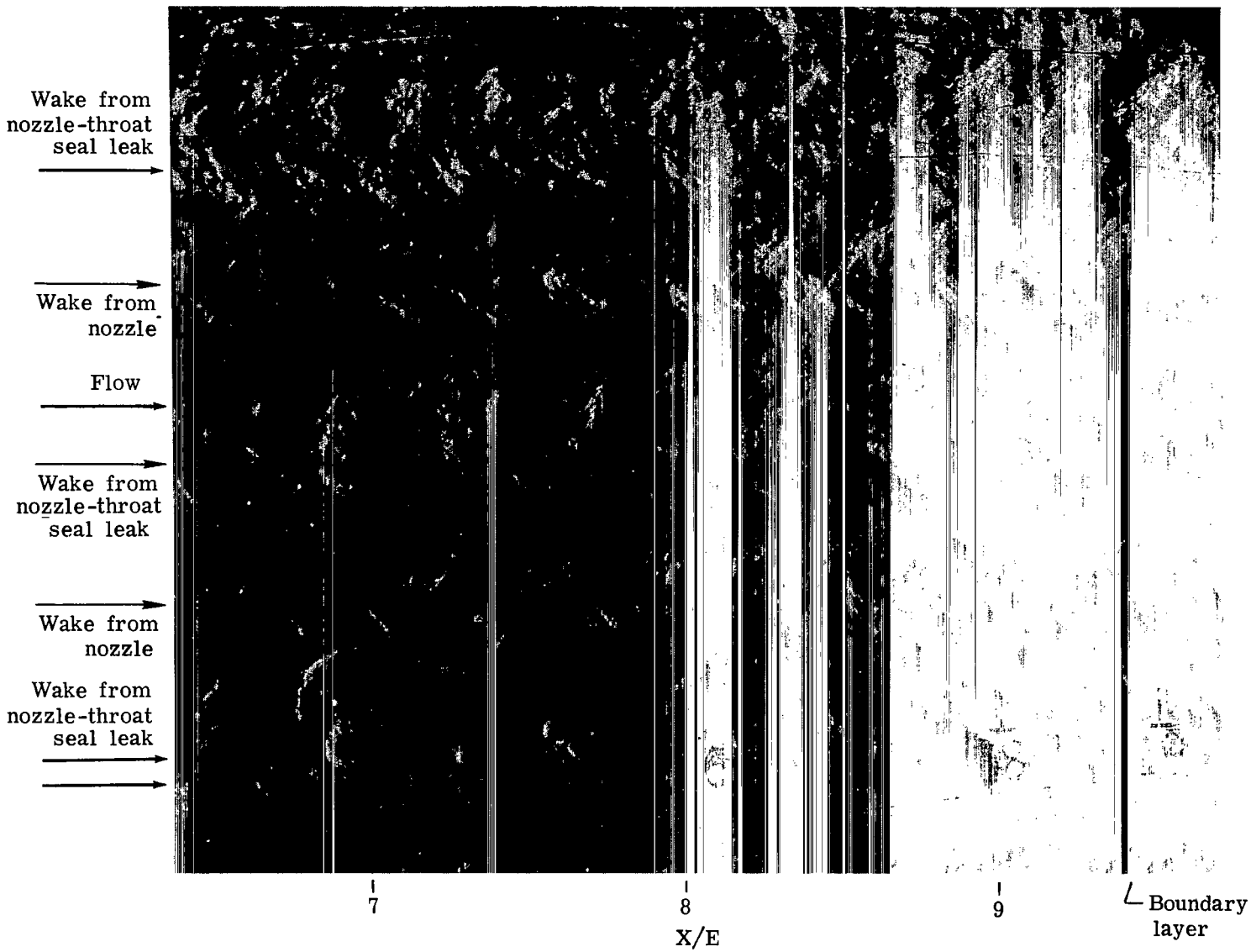

Figure 8.- Shadowgraph of duct flow. Air-gap spark source. Shock waves are not visible. 32.38 cm (12.75 in.) ≤ X ≤ 49.40 cm (19.45 in.).

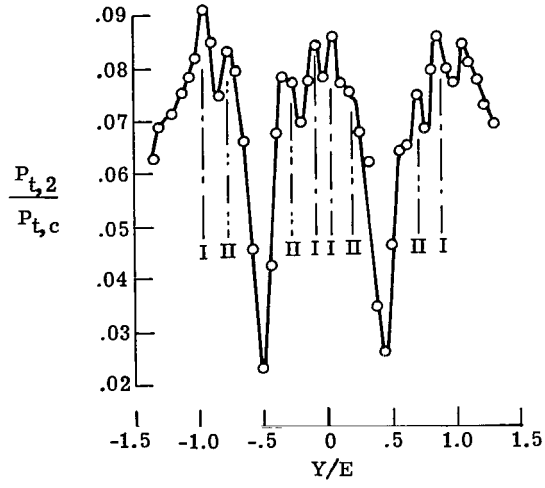

(a) X/E = 1.38.

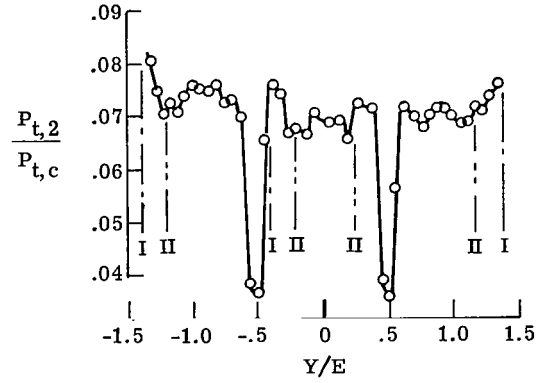

(b) X/E = 3.25.

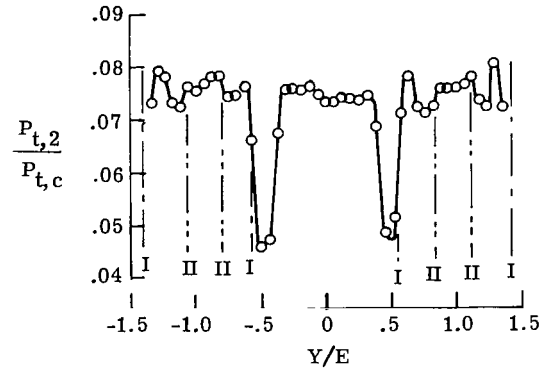

(c) X/E = 7.16.

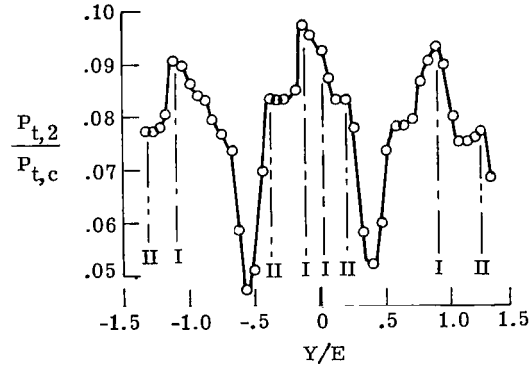

(d) X/E = 9.16.

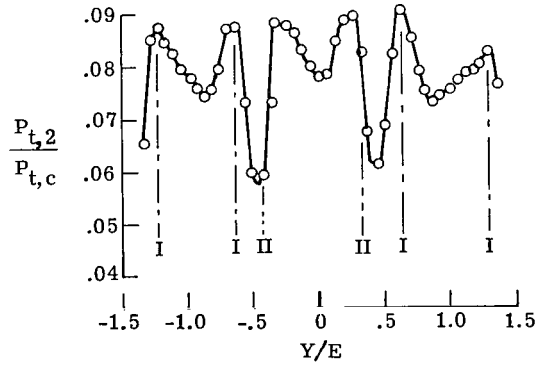

(e) X/E = 11.66.

Figure 9.- Pitot pressure variation at five axial stations in the duct. $P_{t,c}$ = 586 kPa (85 psia).

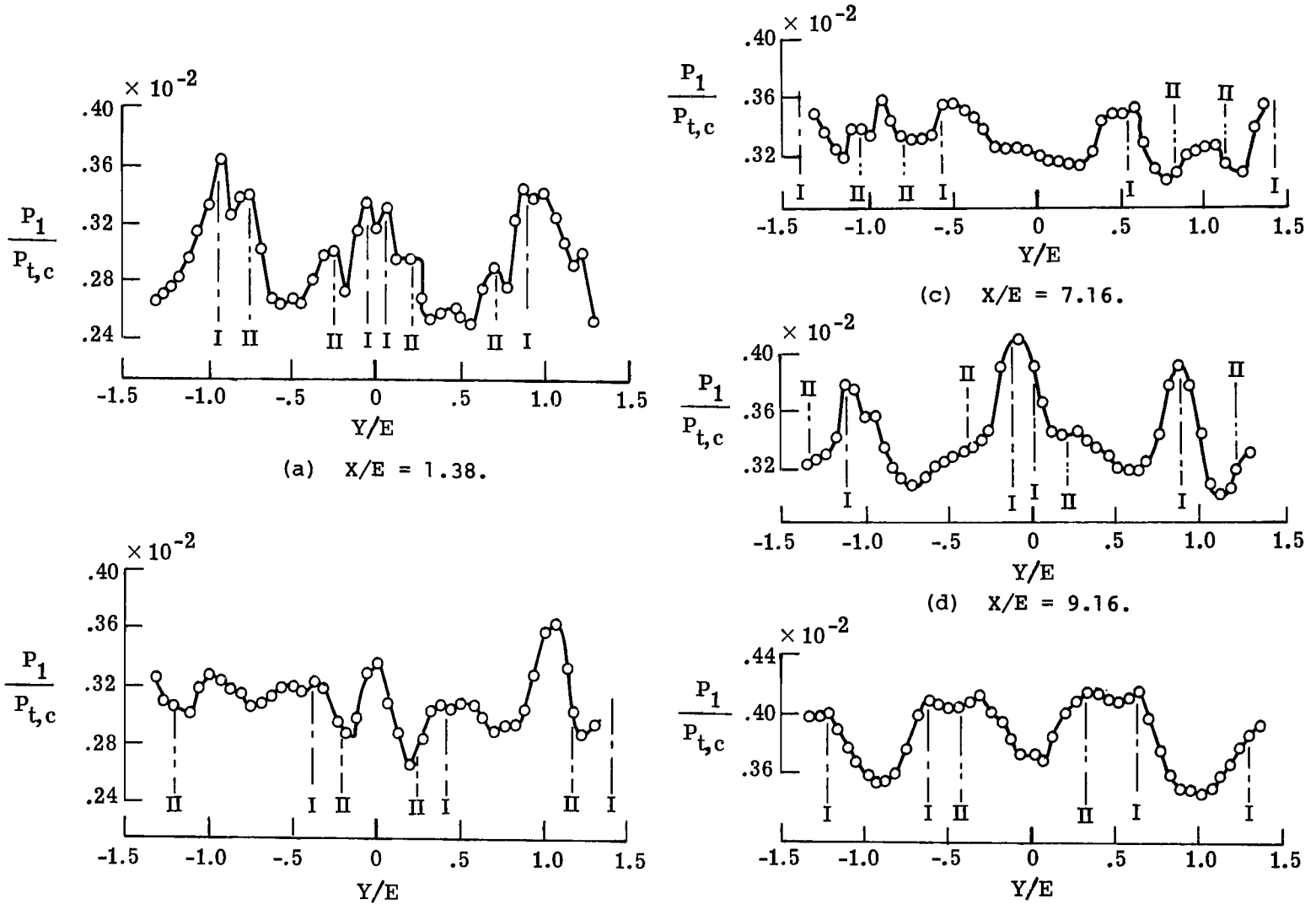

Figure 10.- Static pressure variation at five axial stations in the duct. $P_{t,c}$ = 586 kPa (85 psia).

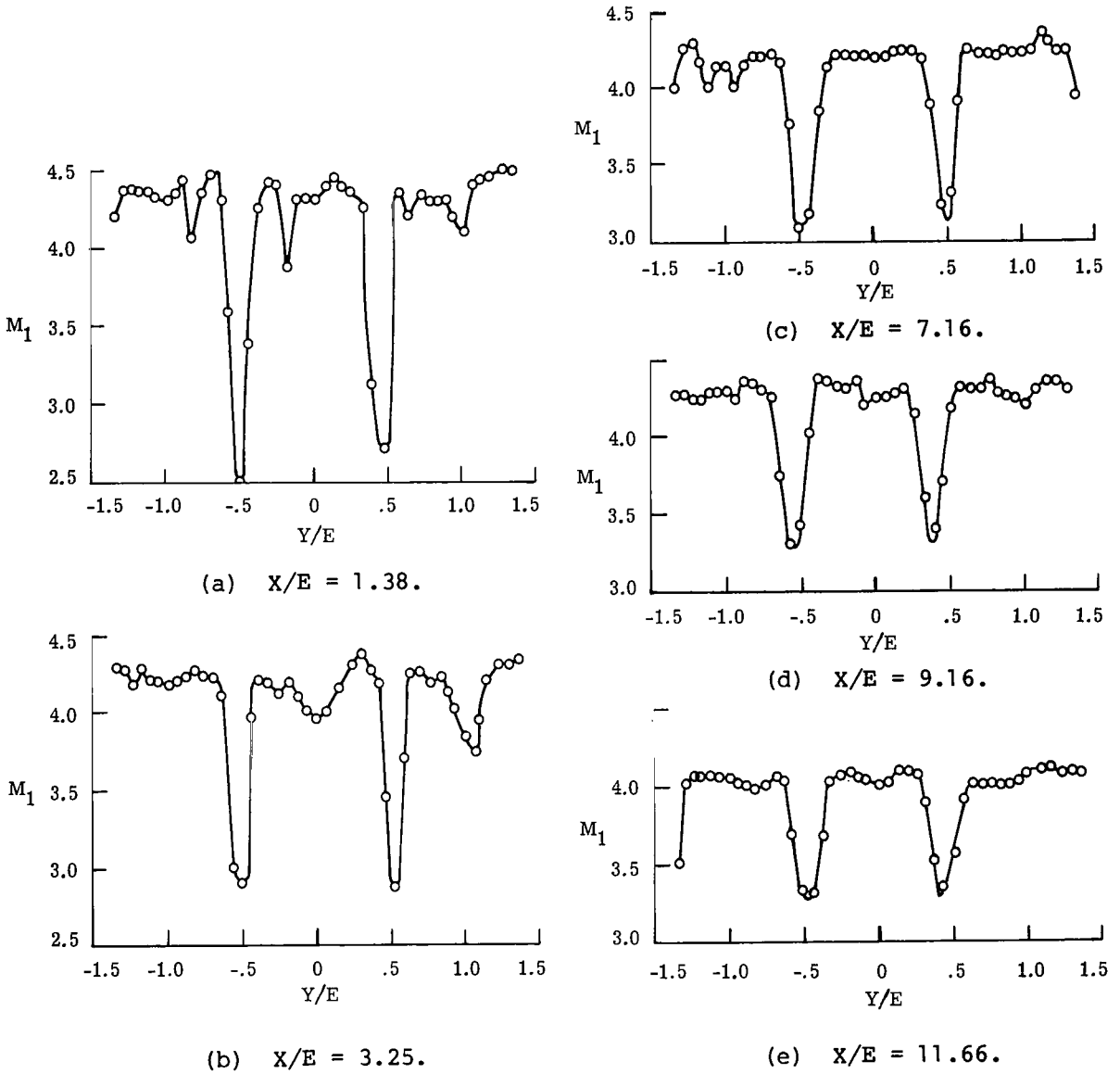

Figure 11.- Mach number variation at five axial stations in the duct.

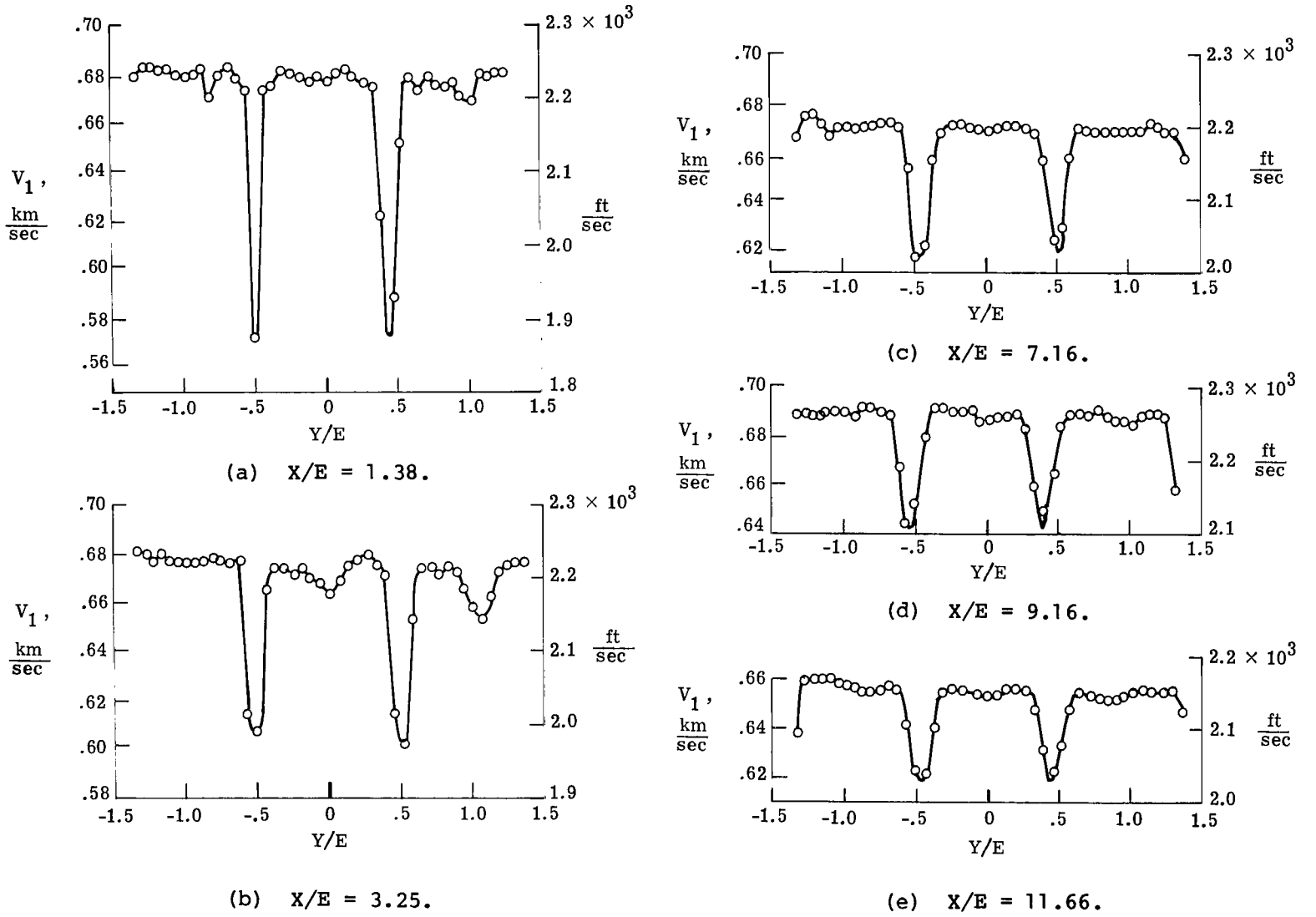

Figure 12.- Velocity variations at five axial stations in the duct.

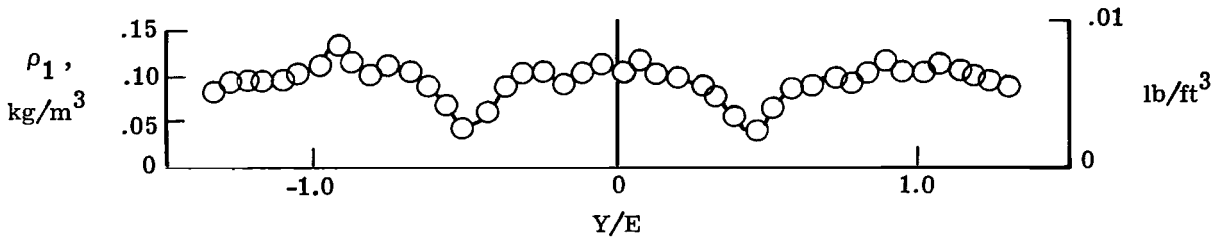

(a) X/E = 1.38.

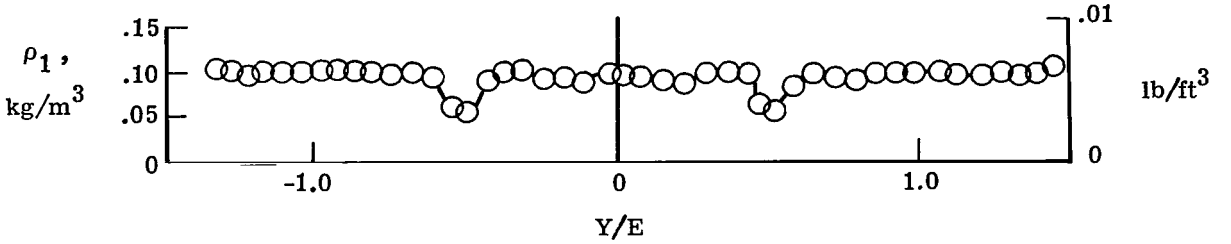

(b) X/E = 3.25.

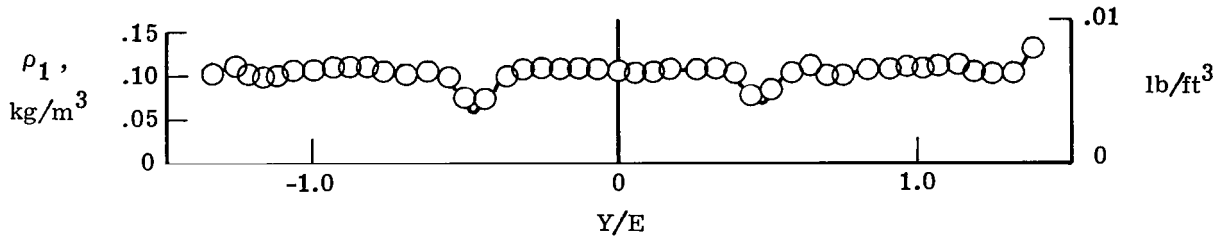

(c) X/E = 7.16.

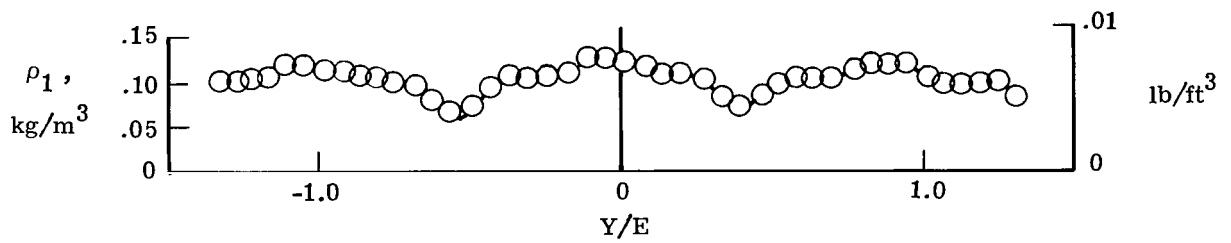

(d) X/E = 9.16.

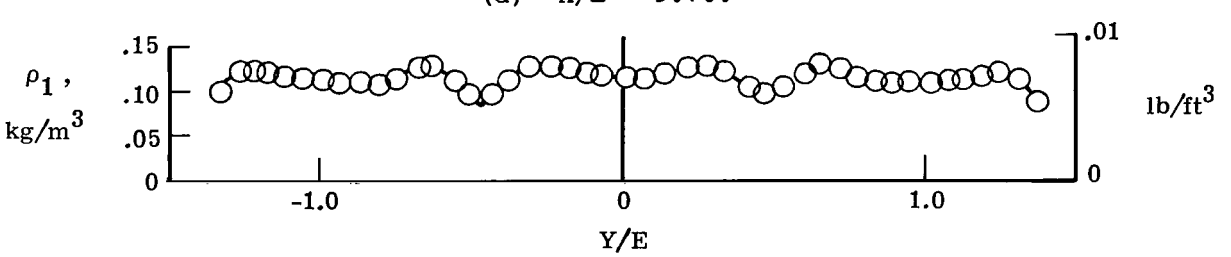

(e) X/E = 11.66.

Figure 13.- Density variations at five axial stations in the duct.

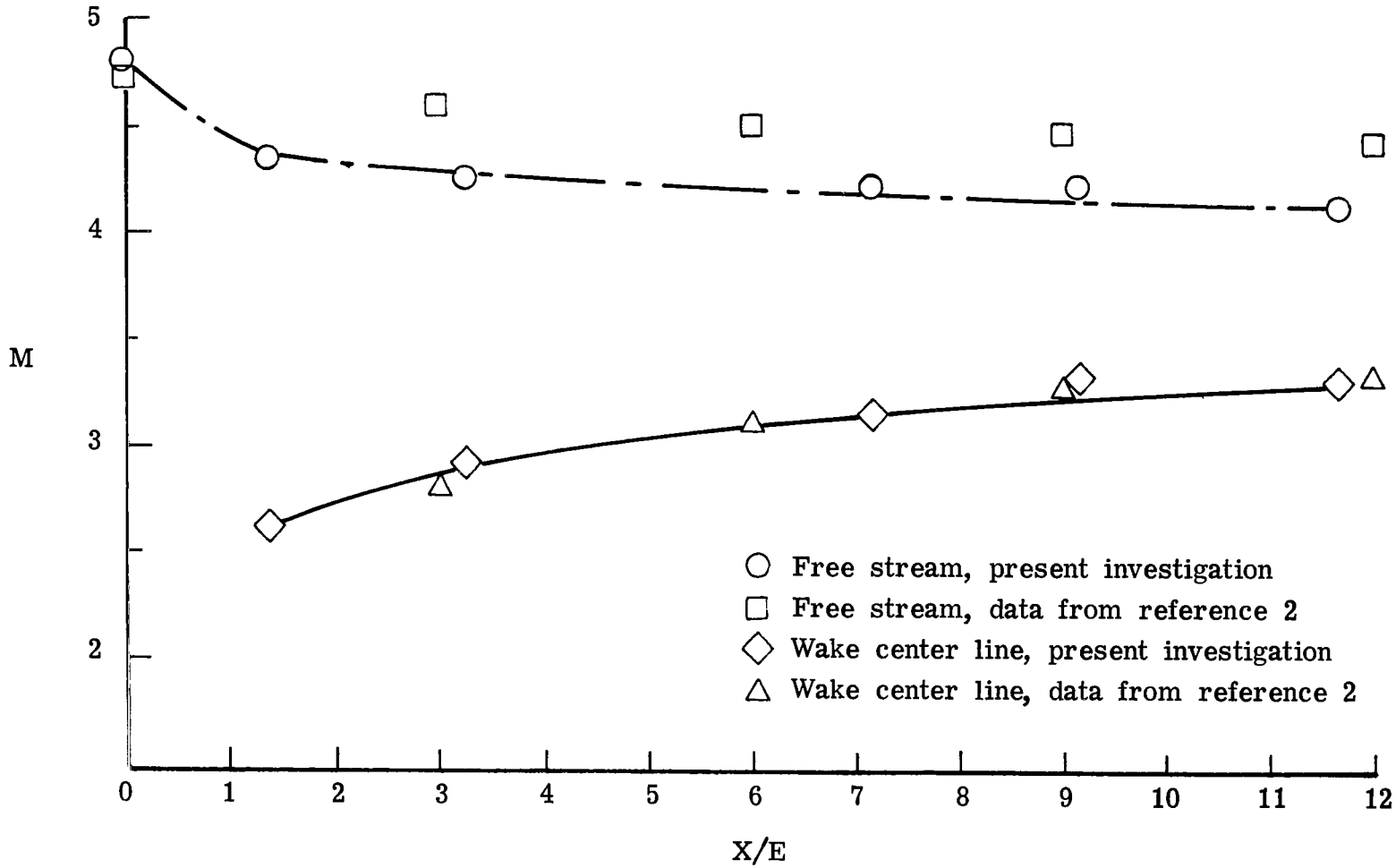

Figure 14.- Axial Mach number variation.

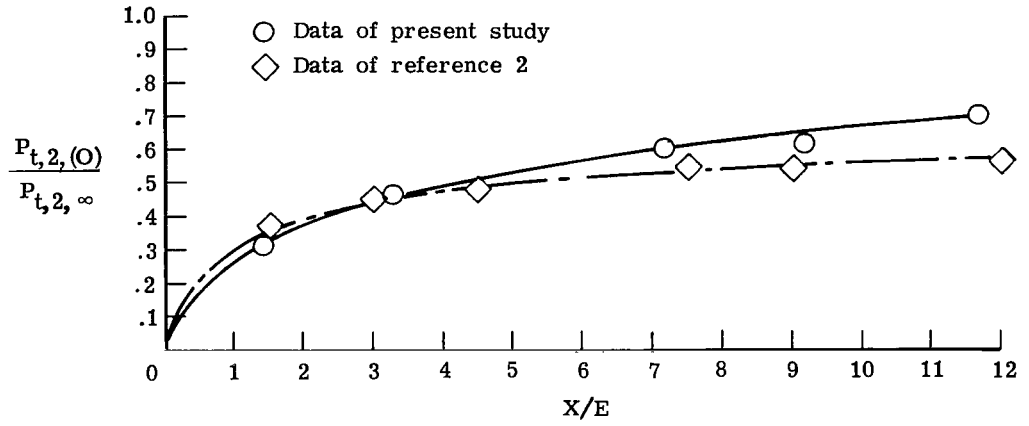

Figure 15.- Axial variation of wake strength.

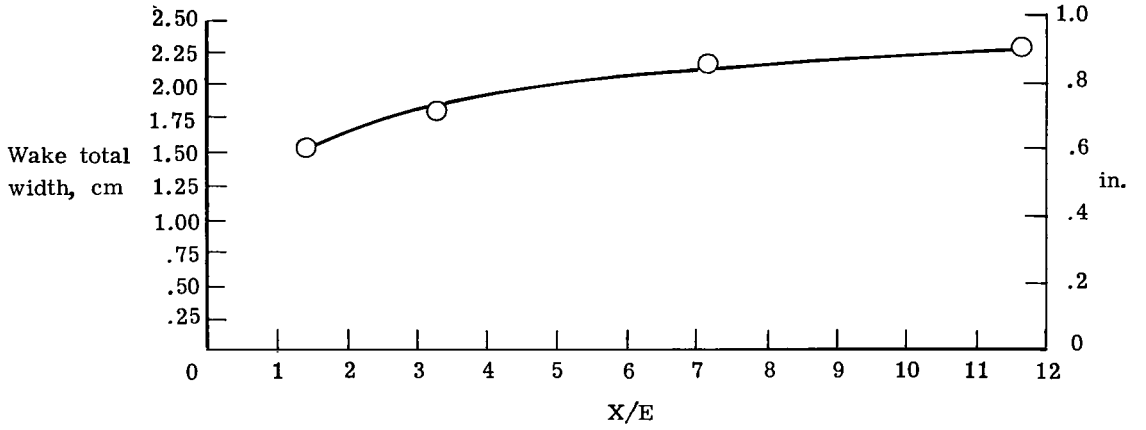

Figure 16.- Axial variation of wake width.

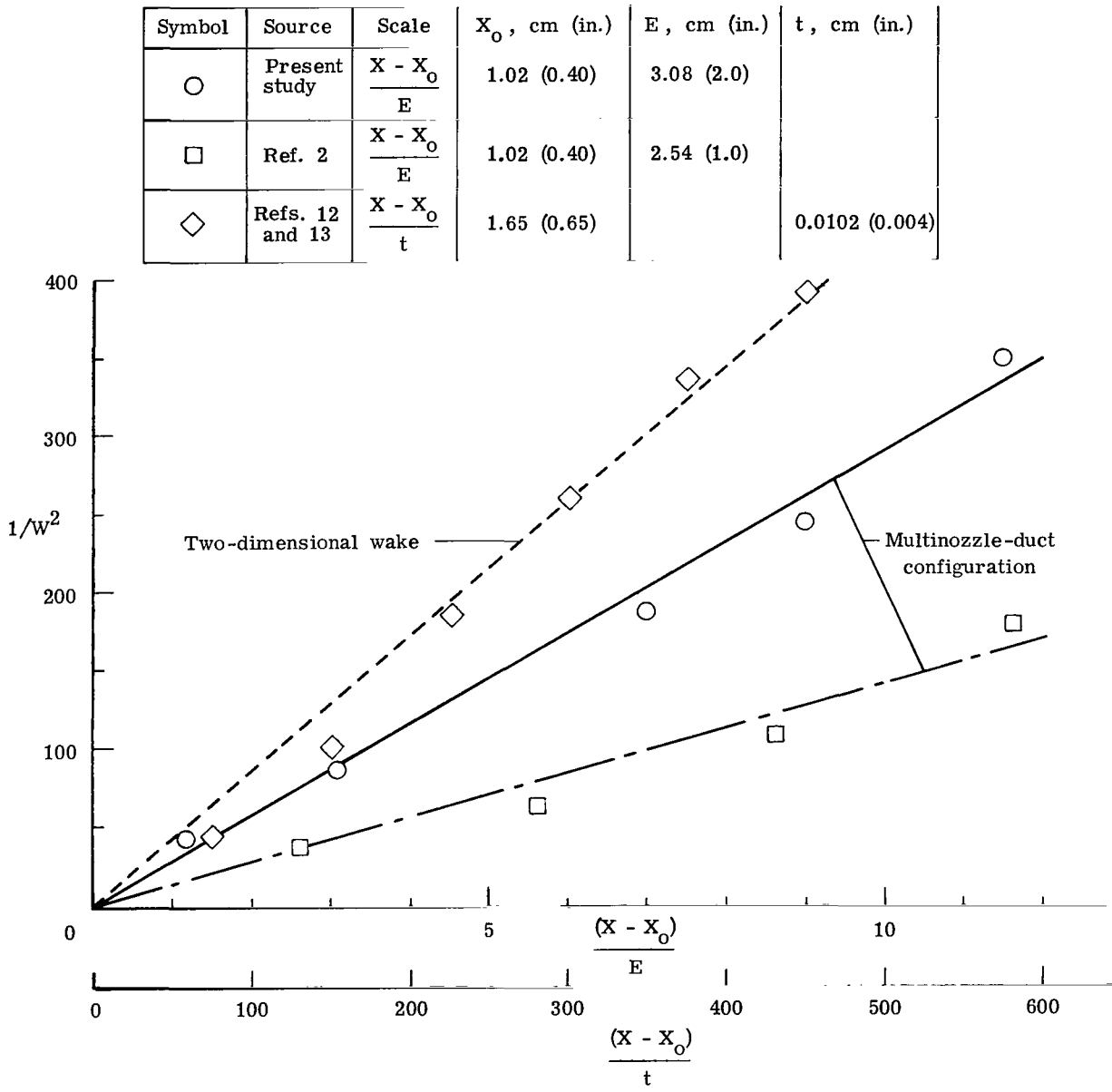

Figure 17.- Normalized axial variation of $1/W^2$ along the wake.

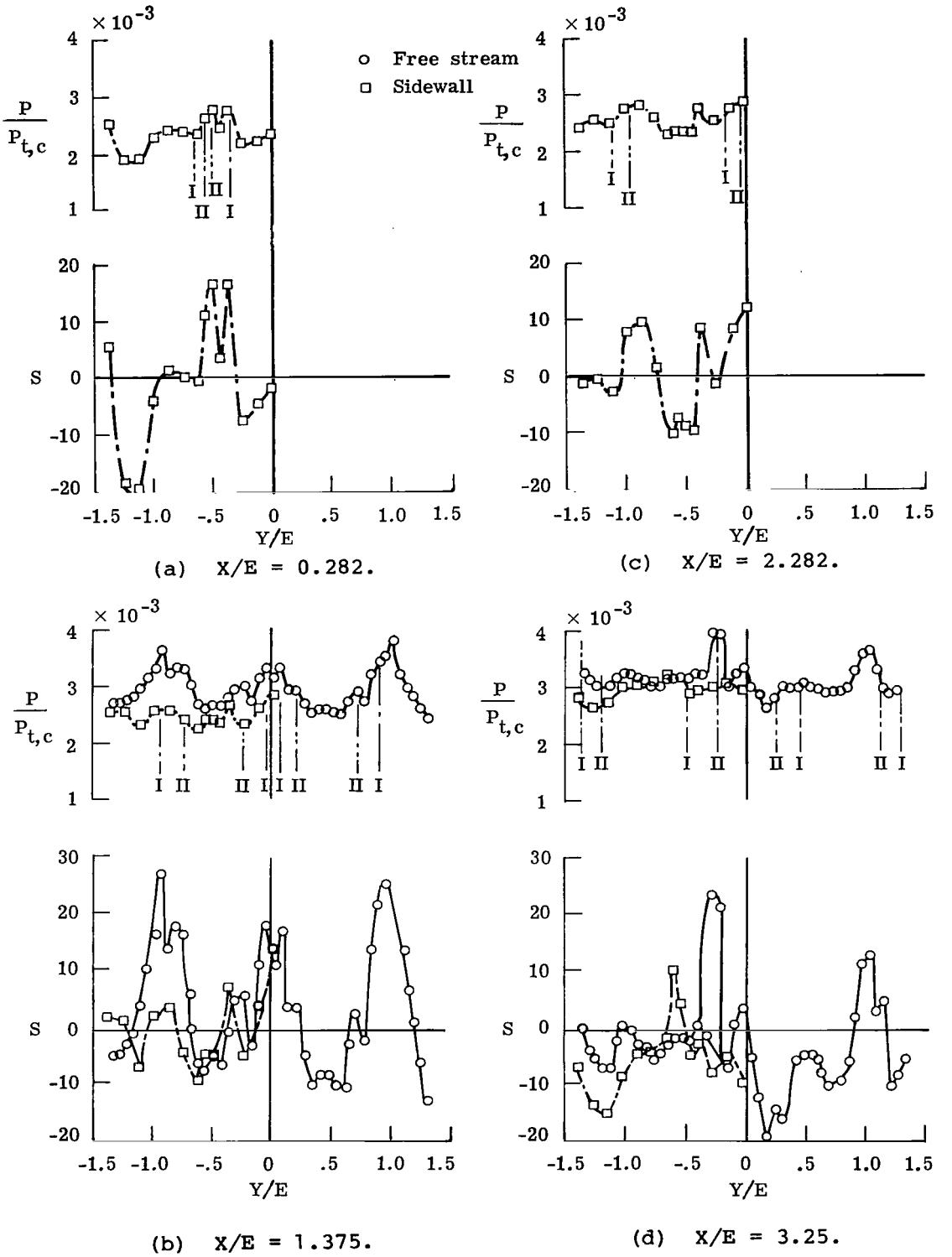

Figure 18.- Duct-sidewall pressure variation with vertical distance.

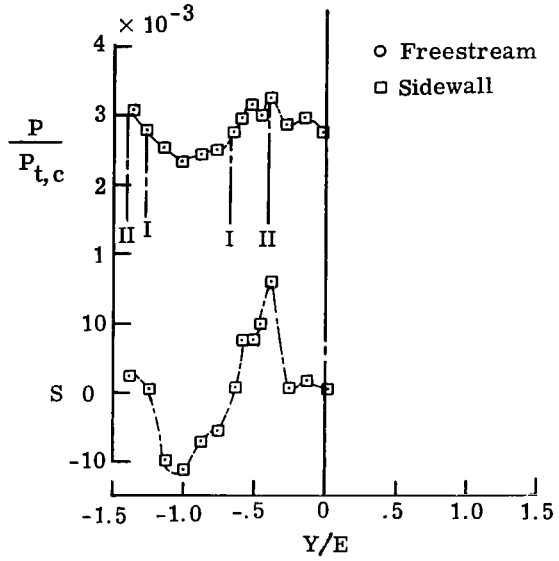

(e) X/E = 4.13.

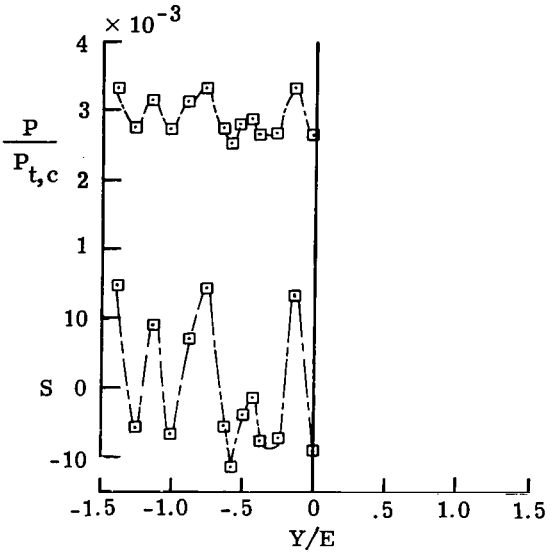

(g) X/E = 6.25.

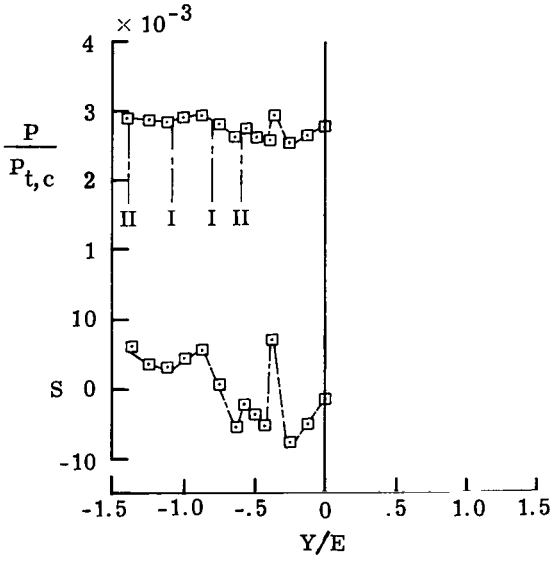

(f) X/E = 4.78.

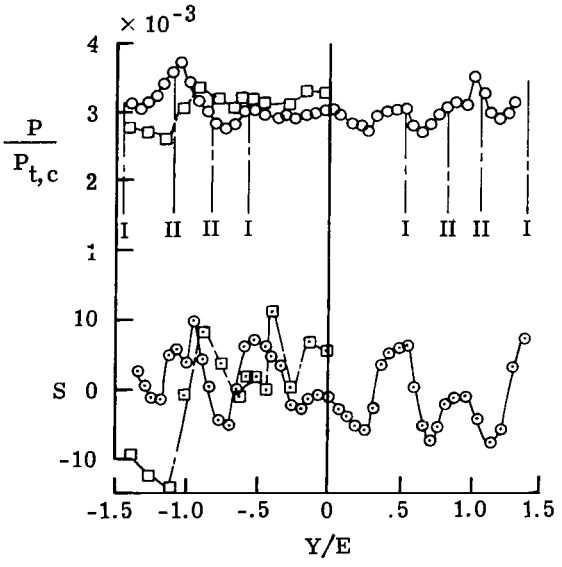

(h) X/E = 7.16.

Figure 18.- Continued.

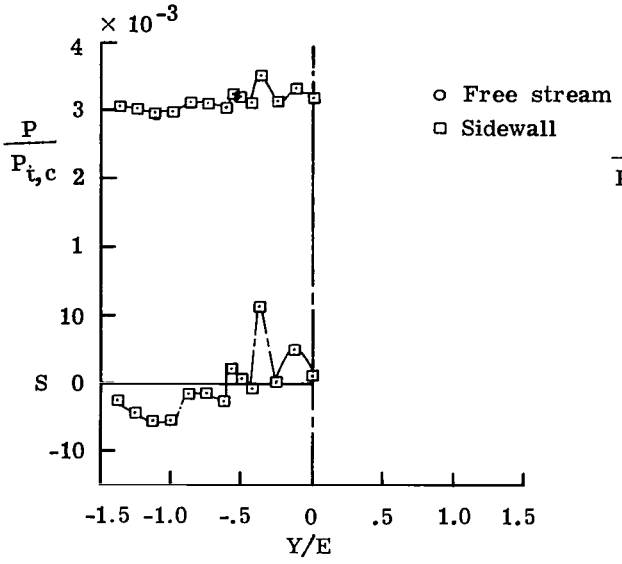

(i) X/E = 8.25.

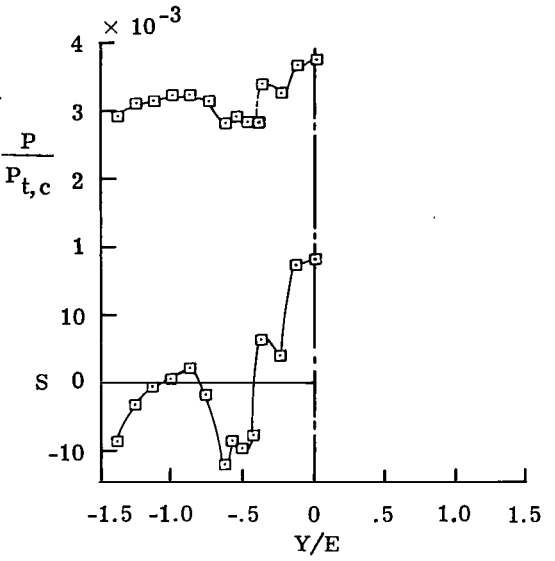

(k) X/E = 10.25.

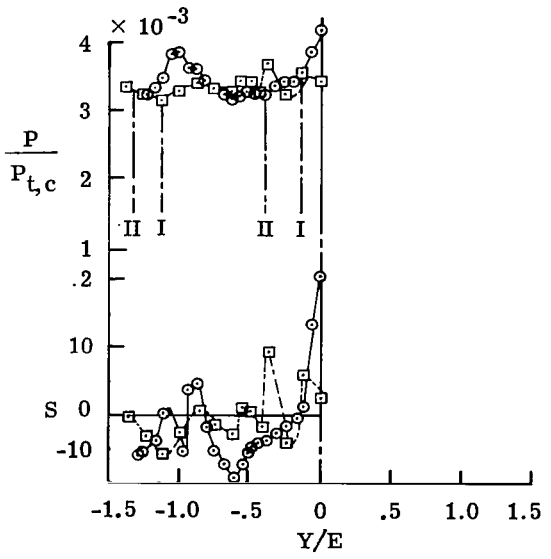

(j) X/E = 9.16.

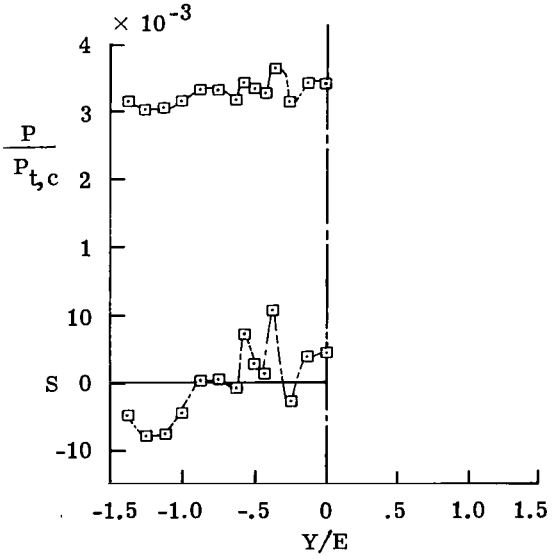

(l) X/E = 11.0.

Figure 18.- Continued.

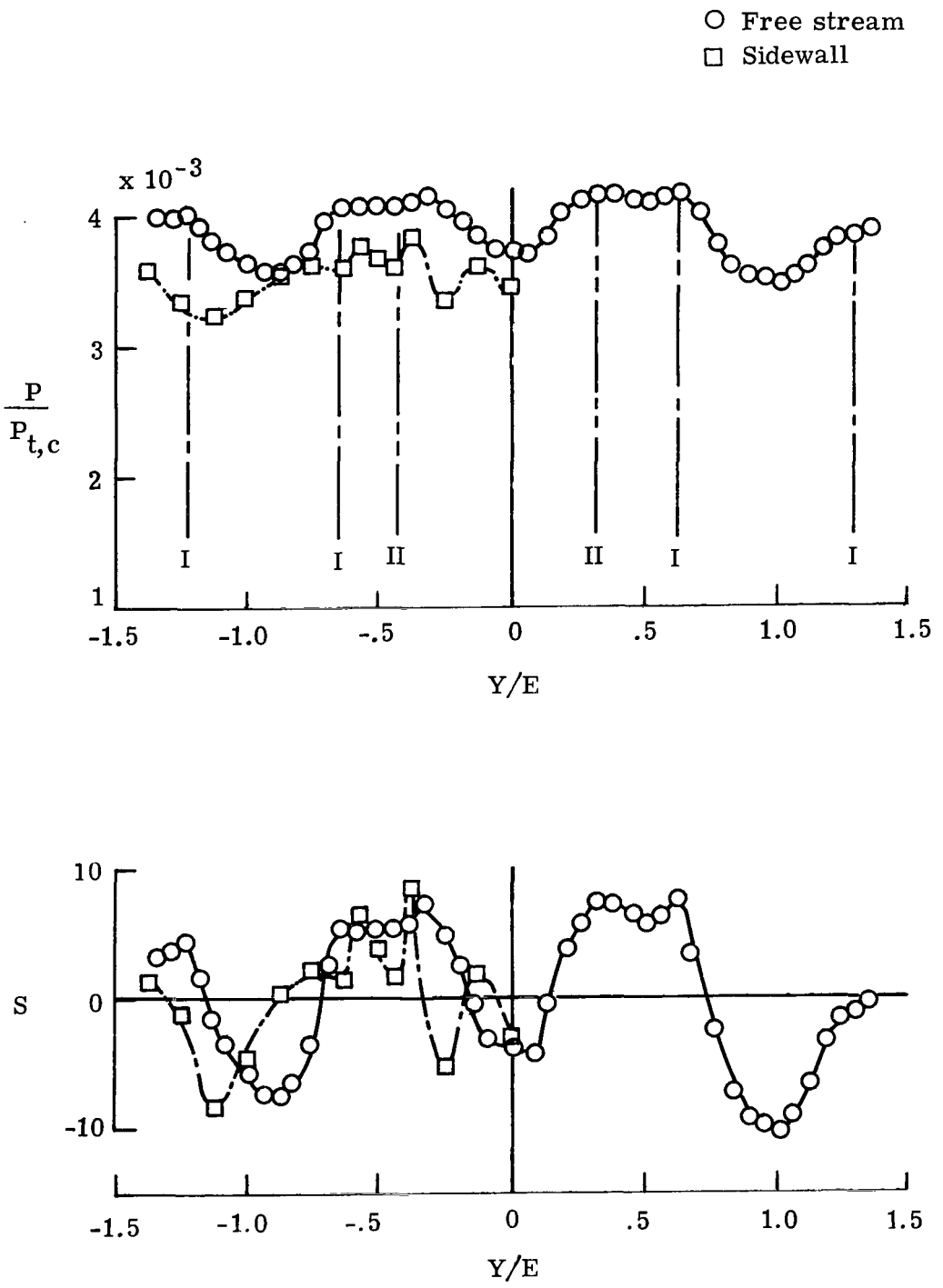

(m) X/E = 11.66.

Figure 18.- Concluded.

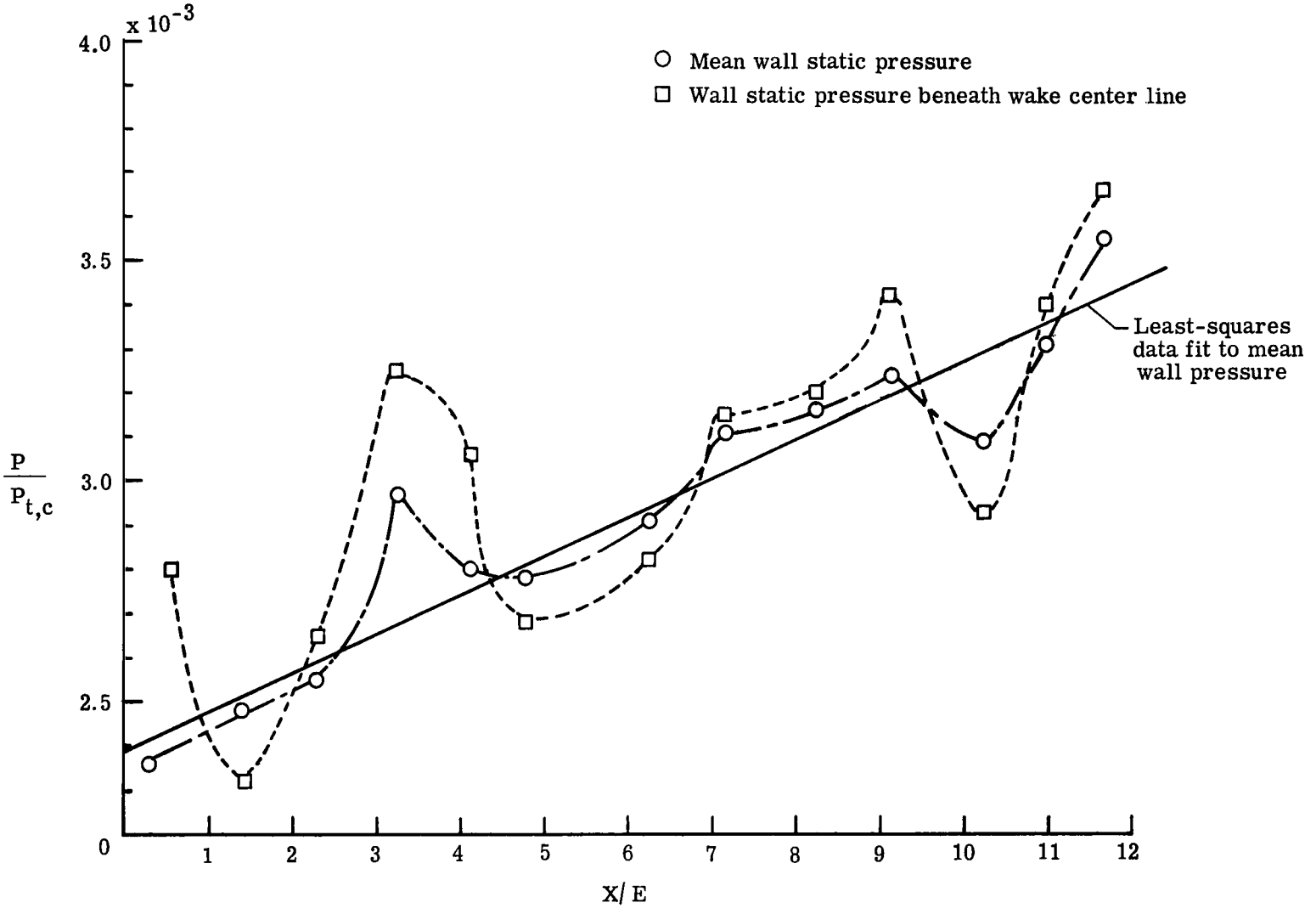

Figure 19.- Duct-sidewall pressure variation with axial distance.

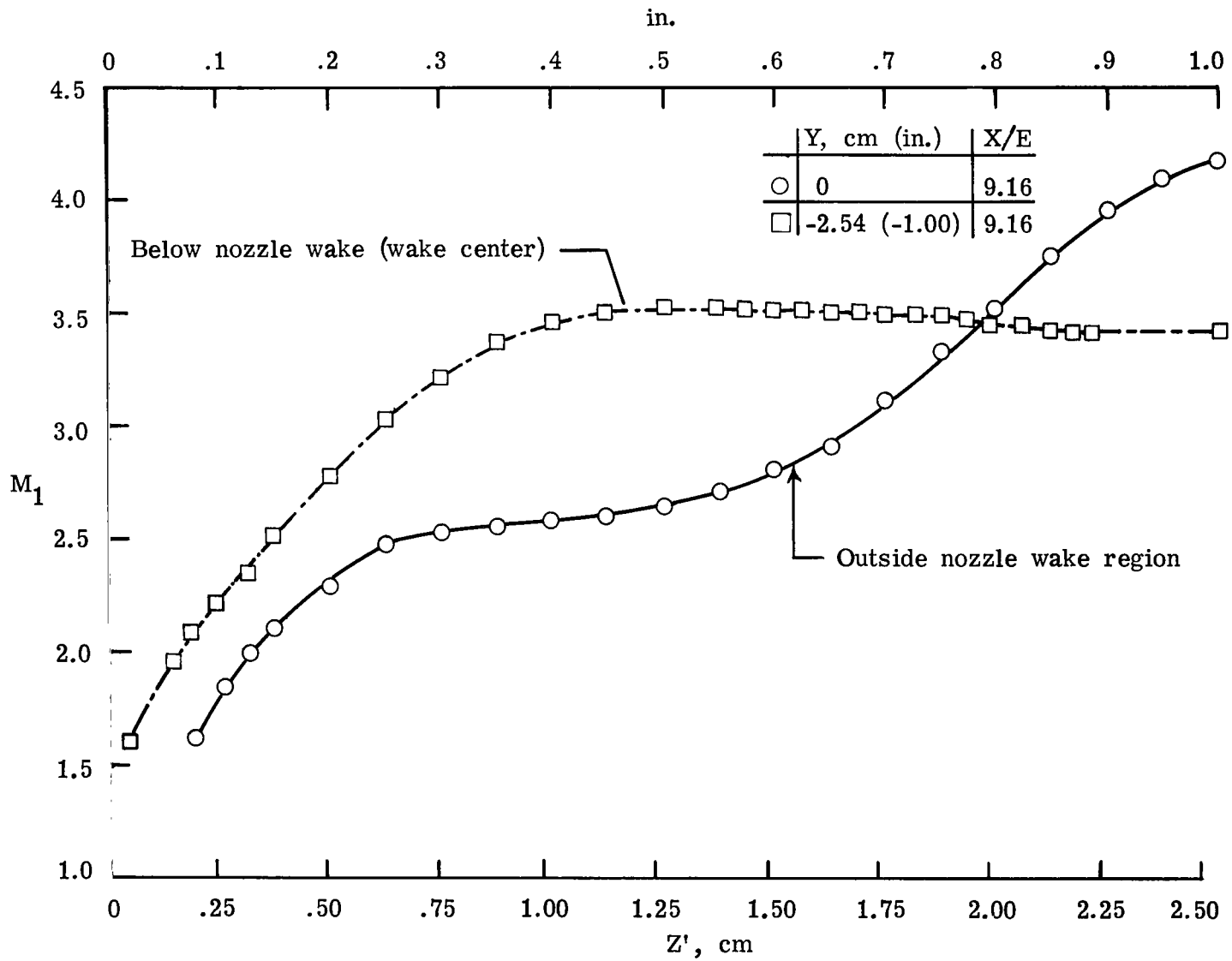

Figure 20.- Mach number profile normal to sidewall.

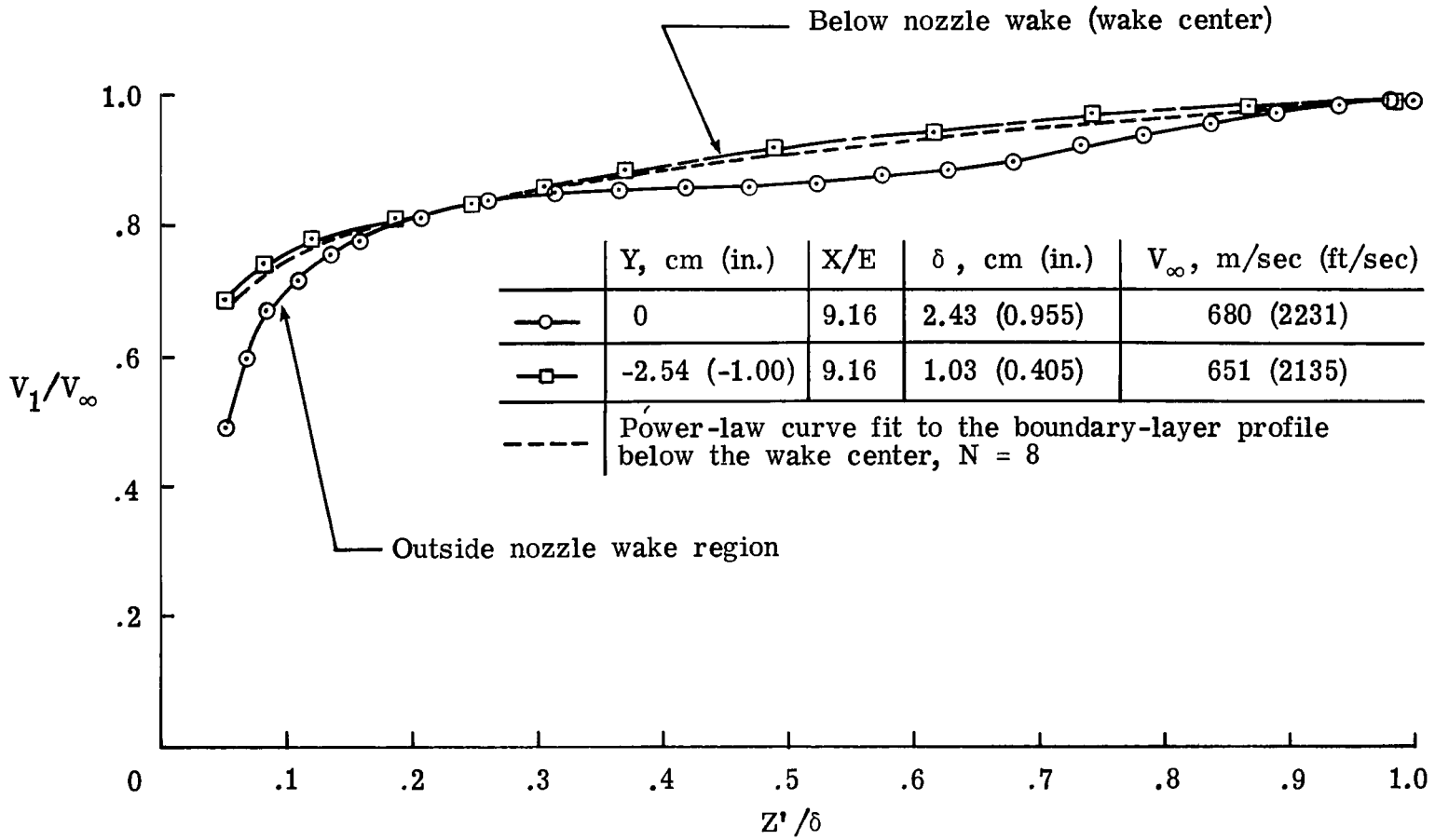

Figure 21.- Velocity distribution normal to sidewall.

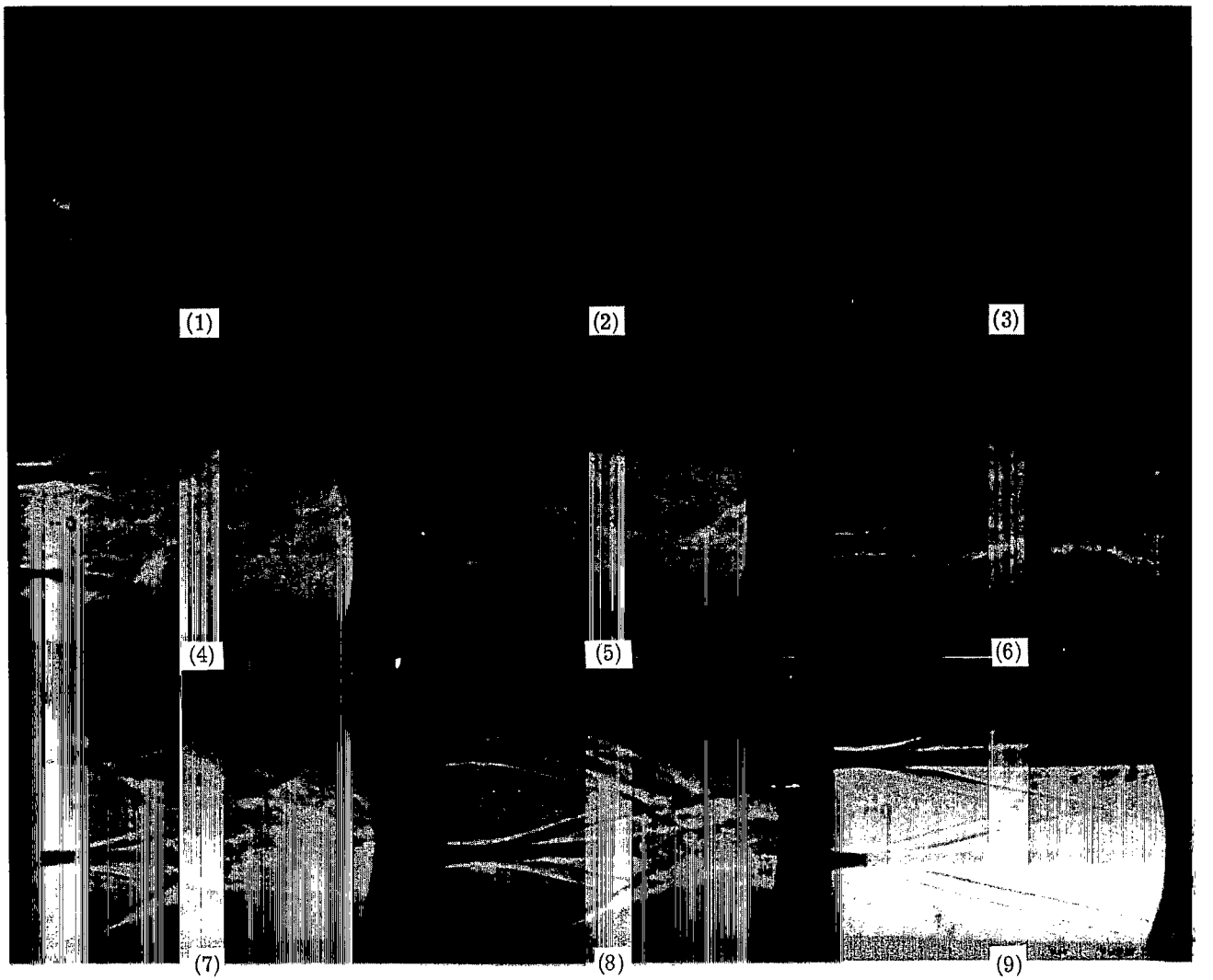

L-78-152

Figure 22.- Start of multinozzle and duct, focused shadowgraph, xenon, light source. -1.91 cm (-0.75 in.) $\leqq$ X $\leqq$ 14.71 cm (5.79 in.).

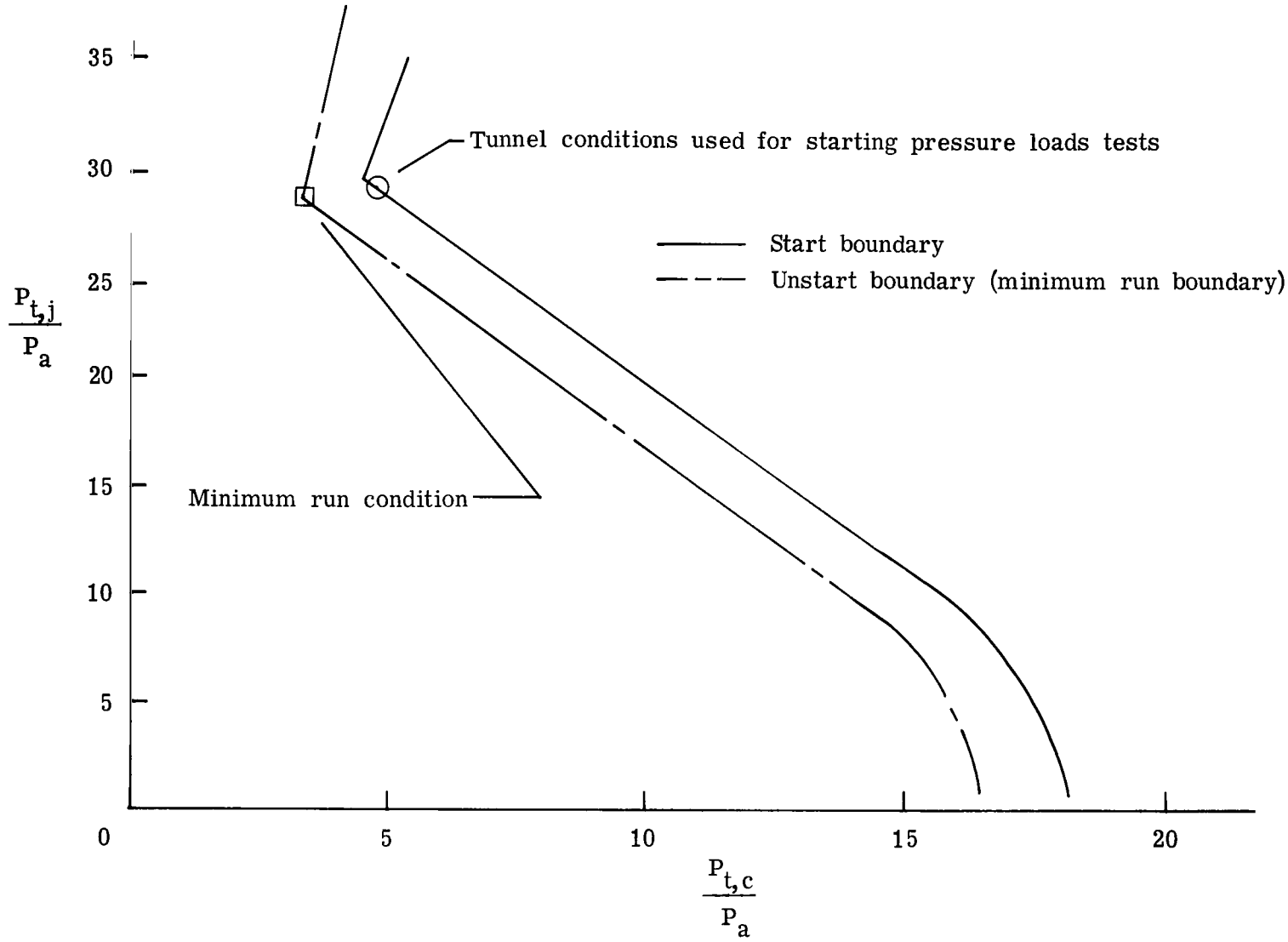

Figure 23.- Wind-tunnel operational range.

1. Report No.	2. Government Accession No.	3. Recipient's Catalog No.
NASA TP-1319		

4. Title and Subtitle
EXPERIMENTAL EVALUATION OF A PILOT MULTINOZZLE-DUCT APPARATUS

5. Report Date
February 1979

6. Performing Organization Code

7. Author(s)
Richard L. Puster

8. Performing Organization Report No.
L-12282

9. Performing Organization Name and Address
NASA Langley Research Center
Hampton, VA 23665

10. Work Unit No.
506-17-43-05

11. Contract or Grant No.

12. Sponsoring Agency Name and Address
National Aeronautics and Space Administration
Washington, DC 20546

13. Type of Report and Period Covered
Technical Paper

14. Army Project No.

15. Supplementary Notes

16. Abstract

A pilot multinozzle and duct were tested at ambient enthalpy to evaluate the suitability of such apparatus for testing thermal protection system (TPS) panels mounted in the sidewalls of the duct downstream of the nozzle array. The flow field in the duct was complex: effects of wakes and shock waves from the nozzles dominated the flow field; the wakes continually mixed with the surrounding fluid; the boundary layer on the sidewalls of the duct was nonuniform; and near the exit of the duct the sidewall pressure variation was as much as 8.5 percent about the mean wall pressure. Starting loads on the duct walls were higher than those of a similar conventional nozzle and duct. It was concluded that the multinozzle-duct apparatus was not suitable for testing TPS panels, although the design and flow-field information should be of interest to designers of high-energy gas-dynamic lasers.

17. Key Words (Suggested by Author(s))	18. Distribution Statement
Multiple nozzle (multinozzle) Gasdynamic laser	Unclassified - Unlimited Subject Category 09

19. Security Classif. (of this report)	20. Security Classif. (of this page)	21. No. of Pages	22. Price*
Unclassified	Unclassified	43	$4.50

*For sale by the National Technical Information Service, Springfield, Virginia 22161

NASA-Langley, 1979

2 1 1U,A, 121278 S00903DS
DEPT OF THE AIR FORCE
AF WEAPONS LABORATORY
ATTN: TECHNICAL LIBRARY (SUL)
KIRTLAND AFB NM 87117